Investigation of the Network Inhomogeneity of Thiol-Ene Organogels

Doctoral Thesis

(Dissertation)

to be awarded the degree

Doctor rerum naturalium (Dr. rer. nat.)

submitted by

Volkan Can

from Istanbul

Approved by the Faculty of Natural and Materials Sciences

Clausthal University of Technology

Date of Oral Examination

27.09.2013

This thesis was written at the Institute of Physical Chemistry at Clausthal University of Technology, Clausthal-Zellerfeld, Germany, in the time between June 2009 and July 2013

Chair Person of the Board of Examiners
Prof. Dr. Sabine Beuermann

Chief Reviewer
Prof. Dr. Wilhelm Oppermann

Reviewer
Pd. Dr. Jörg Adams

Name, Vorname: **Datum:**
Can, Volkan **16.07.2013**

EIDESSTATTLICHE ERKLÄRUNG

**Hiermit erkläre ich an Eides Statt, dass ich die bei der Fakultät für Natur- und
Materialwissenschaften der Technischen Universität Clausthal eingereichte Dissertation selbständig und ohne unerlaubte Hilfe verfasst und die benutzten Hilfsmittel vollständig angegeben habe.**

Unterschrift

Name, Vorname: **Datum:**
Can, Volkan **16.07.2013**

EIDESSTATTLICHE ERKLÄRUNG

Hiermit erkläre ich an Eides Statt, dass die eingereichte Dissertation weder in Teilen noch in ihrer Gesamtheit einer anderen Hochschule zur Begutachtung vorliegt oder vorgelegen hat und dass ich bisher noch keinen Promotionsversuch unternommen habe.

Unterschrift

ACKNOWLEDGEMENTS

First of all, I want to thank **Professor Dr. Wilhelm Oppermann** for the support and the opportunity of free way of thinking that he provided at the same time. His guidence helped me get through this study. I also want to thank to **Dr. Jörg Adams** for reviewing my thesis and helpful advises during my study.

I would like to thank **Carina Hallensleben, Chris Fruhner, Tetjana Laba, Frederik Droste-Rehling, Marco Tapken, Tobias Grimm, Robert König** for their contribution to this study.

I want to express my gratitude to **Arne Langhoff** for his endless support, valuable discussions and friendship.

I also owe many thanks to **Arne Langhoff, Svenja Grube** and **Deniz Tuncaboylu** for reviewing my dissertation,

Michael Tölle for being always positive and providing all the essential equipments in the most helpful manner and,

Andrea Kornhard for not complaining even once when I knocked her door and providing her help sincerely.

I also want to thank **Svenja Grube, Katja Pohl, Stefanie Helga Maria Telsemeyer-Schauer, Azadeh Raeisi, Anne Hagge, Sylvia Hanke, Robert Scherf, Rebekka König, Nadine Kruse, Annika König, Alexander König, Markus Sussoff, Julia Gansel, Eike Hübner, Neena Christiansen, Tim Wang, Antje Britze** and **all my collegues in the Institute of Physical Chemistry** for their help to adjust myself to a new culture, friendliest atmosphere and the joy that they brought to the working environment,

To **Saadet Dogu** and **Ayse Ertekin** for sharing the troubled moments of the life in this small “city” as well as the pleasant ones,

To **Bilge Kilic, Savas Sagman** and **Faruk Ozkan** for their true friendship,

To **Gökhan Temel, Deniz Corabatir, Koray Yilmaz, Deniz Tuncaboylu** and **Murat Gulcur** for being the best buddies for life,

To **Oguz Okay, Nermin Orakdogen** and **Suzan Abdurrahmanoglu** for their wisdom,

To **Ilker Akmirza** and **Kagan Utku Can** for always being there,

And ofcourse to **MY FAMILY** for their endless support, understanding...

Thank You All !!!

ABSTRACT

Thiol-ene networks were synthesized at different monomer concentrations by using difunctional triethyleneglycol divinylether monomer and tetrafunctional pentaerithritol trimercaptopropionate crosslinker. The studied network is thought to have a homogenous structure due to the stepgrowth nature of the polymerization mechanism during synthesis. The aim of this thesis was to investigate this idea with the help of various methods such as rheology and dynamic light scattering.

Measurements are conducted during and after synthesis of thiol-ene networks. Rheological measurements showed that the gelation reaction via the thiol-ene mechanism is quite rapid and the gels synthesized have a relatively high crosslinking efficiency up to 60% with respect to the predictions of phantom network model. This was explained by the high monomer conversion at the gel point. Syneresis is observed for the networks below 20% (w/v) monomer concentration due to the contraction of the network as the clusters merge during the crosslinking reaction.

DLS measurements were conducted with networks right after the synthesis and in equilibrium swollen states. Applying the nonergodic approach according to Pusey and van Megen, the static portion of the ensemble average scattering intensity was found to be 90±2% for concentrations 10% (w/v) and above. Compared to the measurements conducted right after synthesis, the ensemble average scattering intensity is also found to increase up to 25 fold as the gel reaches to equilibrium swollen state, which uncovers the inhomogenous nature of the thiol-ene networks.

TABLE OF CONTENTS

1 INTRODUCTION

Polymeric gels are three-dimensional networks of polymer chains that are connected with chemical and/or physical crosslinks and which are swollen in a solvent. They have a wide range of practical applications such as biomaterials, sensors and super absorbents [1-5]. Since the nature and the formation mechanism of the network bonds strictly affects the properties of these materials, [6-7] it is worth investigating the relationship between the macrostructure and the microstructure inside the network.

Homogeneity is one of the most desired properties of polymer networks to obtain mechanically strong, optically transparent polymeric gels. Many approaches are developed in order to obtain homogeneous polymer networks such as application of controlled polymerization techniques, introducing monomers with bulky side groups, or crosslinking polymer solutions [8-10]. Among the existing techniques, thiol-ene polymerization is getting favorable in the last two decades due to the practical advantages such as non-sensitivity to oxygen, low shrinkage during the synthesis and high number of possible reactants which provides a structural variety [11]. Furthermore, since thiol-ene polymerization proceeds via radicalic step-growth mechanism, gelation occurs at high monomer conversions compared to conventional free radical crosslinking copolymerization, leading to more homogeneous networks [12-13].

However the studies investigating the structure-property relationship of these materials are mostly limited to bulk resins, and there are not enough studies on the properties of thiol-ene gels synthesized in the presence of a diluent. Also the microstructure of thiol-ene organogels are not investigated yet with direct methods such as dynamic light scattering.

The main objective of the present study is to investigate the microstructure and inhomogeneity of thiol-ene networks. Dynamic light scattering and rheological techniques are mainly utilized for this purpose.

2 BACKGROUND

2.1 Step Growth Polymerization

Since thiol-ene polymerization proceeds via a step growth polymerization mechanism [11-14], an introduction about this mechanism and its distinctive properties will be given in this chapter. The main reason that this mechanism is called step growth is because it proceeds via stepwise reactions of difunctional monomer pairs.

The most distinctive feature of the step growth polymerization that distinguishes it from the chain growth polymerization is the growth of molecular weight with the conversion. A general scheme of the relationship between molecular weight (M_w) and monomer conversion for both step growth and chain growth polymerization is shown in Scheme 1.

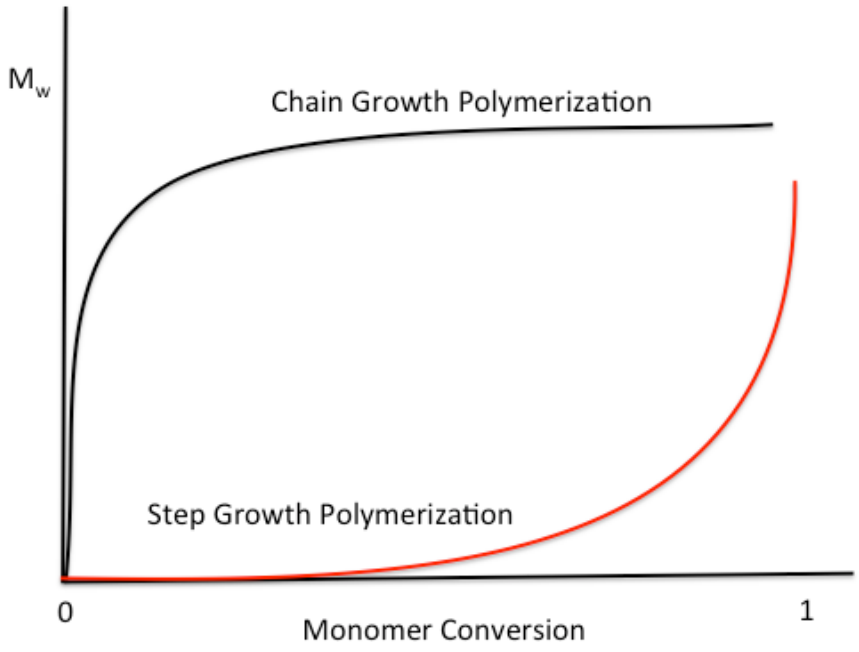

Scheme 1. Growth of molecular weight with respect to monomer conversion during chain growth and step growth mechanism.

This behavior can be explained by using the Carothers equation [15]. For a step growth polymerization the number average degree of polymerization, *DP*, can be expressed as

$$DP = \frac{A_0}{A_t} \qquad (1)$$

where A_0 and A_t are number of molecules at the beginning of the reaction and the number of molecules at time *t,* respectively. If $A_t = A_0(1 - p)$, where *p* is the fraction of functional groups that have reacted at time *t*, and *(1-p)* is the fraction of unreacted functional groups, equation 1 becomes:

$$DP = \frac{A_0}{A_0(1-p)} = \frac{1}{1-p} \qquad (2)$$

which is known as the Carothers equation.

2.2 Thiol-Ene Polymerization

Highly efficient reactions of thiols with reactive carbon-carbon double bonds or so-called “enes” have been known for more than a century now [16-17]. High yields, rapid reaction rates over a large concentration range, being insensitive to ambient oxygen or water and availability of a wide range of both thiols and enes makes this type of reactions quite versatile in a large number of application areas such as dental restorative materials, microfluidic devices, biomaterials or the synthesis of functional polymers [18-22].

An important advantage of thiol-ene reactions is the broad range of monomer choices [11]. For enes, having a non-sterically hindered terminal structure is the only requirement to participate in a thiol-ene polymerization. In general the reactivity of the ene structure increases with the electron density of the carbon-carbon double bond. However, norbornene structure is an exception

while the ring strain increases the reactivity. The following sequence lists various enes in order of decreasing reactivity [11]:

Norbornene > Vinyl ether > Propenyl > Alkene ≈ Vinyl ester > N-vinyl amide > Allyl ether ≈ Allyltriazine > N-vinyl amide > Allyl ether ≈ Allyltriazine ≈ Allylisosyanurate > Acrylate > Unsaturated ester > N-substituted maleimide > Acrylonitrile ≈ Methacrylate > Styrene > Conjugated Dienes

Scheme 2 shows the three types of multifunctional thiols used mostly in thiol-ene photopolymerization reactions : alkyl thiols, thiol glycolate esters and thiol propionate esters. Thiols based on propionate esters and glycolate esters result in greater reaction rates because of a weakening of the sulfur-hydrogen bond by hydrogen bonding of the thiol hydrogen groups with the ester carbonyl.

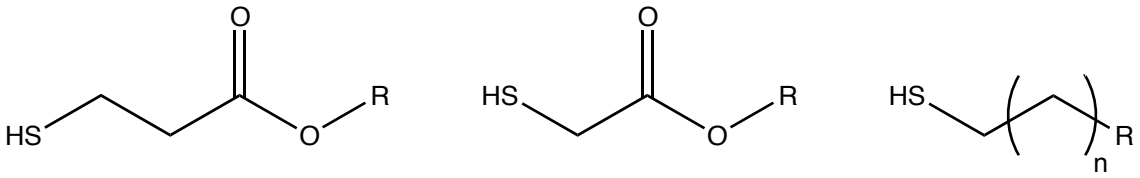

Alkyl 3-mercaptopropionate Alkyl thioglycolate Alkyl thiol

Scheme 2. Most common thiol structures used in thiol-ene photopolymerization reactions. [11]

2.2.1 Thiol-Ene Polymerization Mechanism

Thiol-ene polymerization proceeds by the radically catalyzed addition of a thiol to a vinyl functional group. When multifunctional monomers with an average functionality greater than two are utilized, highly cross-linked polymer networks are formed via a step growth mechanism. As shown in scheme 3, the thiol-ene step growth reaction is initiated with the creation of a radical on the thiol group (step 1). Then propagation takes place via addition of the thiyl radical to a vinyl function (step 2), followed by chain transfer from the resulting

carbon radical to a thiol functional group, regenerating the thiyl radical (step 3). These successive propagation/chain transfer steps serve as the basis for the step growth thiol-ene photopolymerization reaction. Finally, termination occurs by coupling of any two radical species (step 4).

Step 1 – Initiation

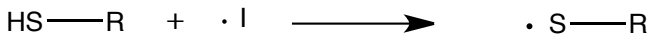

Step 2 – Propagation

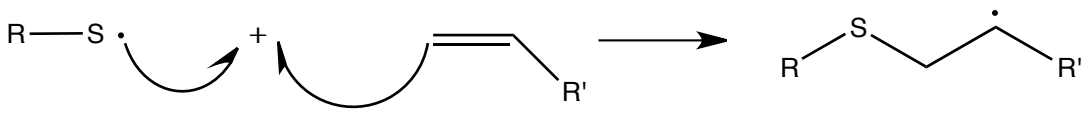

Step 3 – Chain transfer

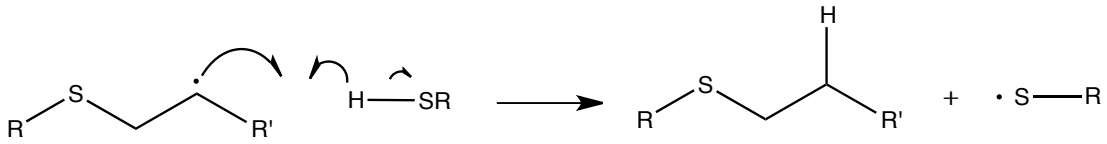

Step 4 – Termination

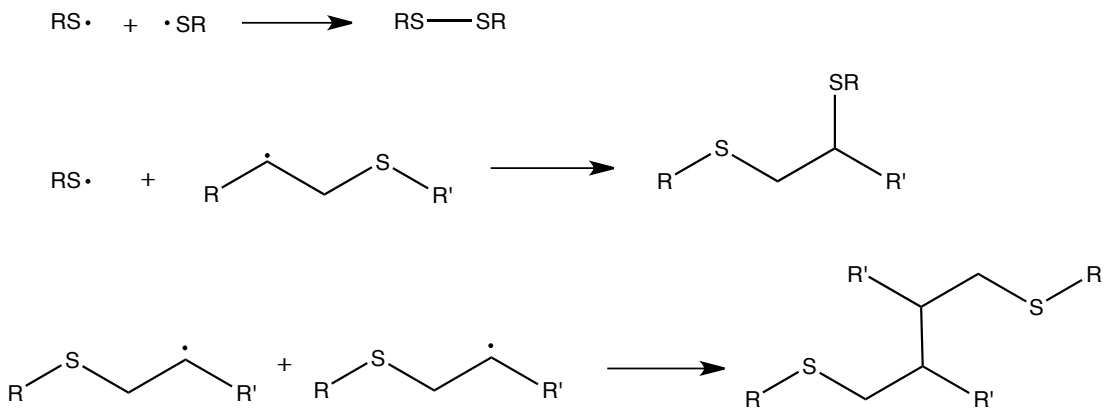

Scheme 3. Mechanism of thiol-ene reaction

2.2.1.1 Oxygen Insensitivity

One of the most favorable properties of the thiol-ene polymerization mechanism is the oxygen insensitivity. As shown in scheme 4, peroxy radicals are created with the presence of oxygen in the system. They do not add to the polymer, but instead, undergo a chain transfer reaction with a thiol to give an oxygen addition product and regenerate the propagating species again [23].

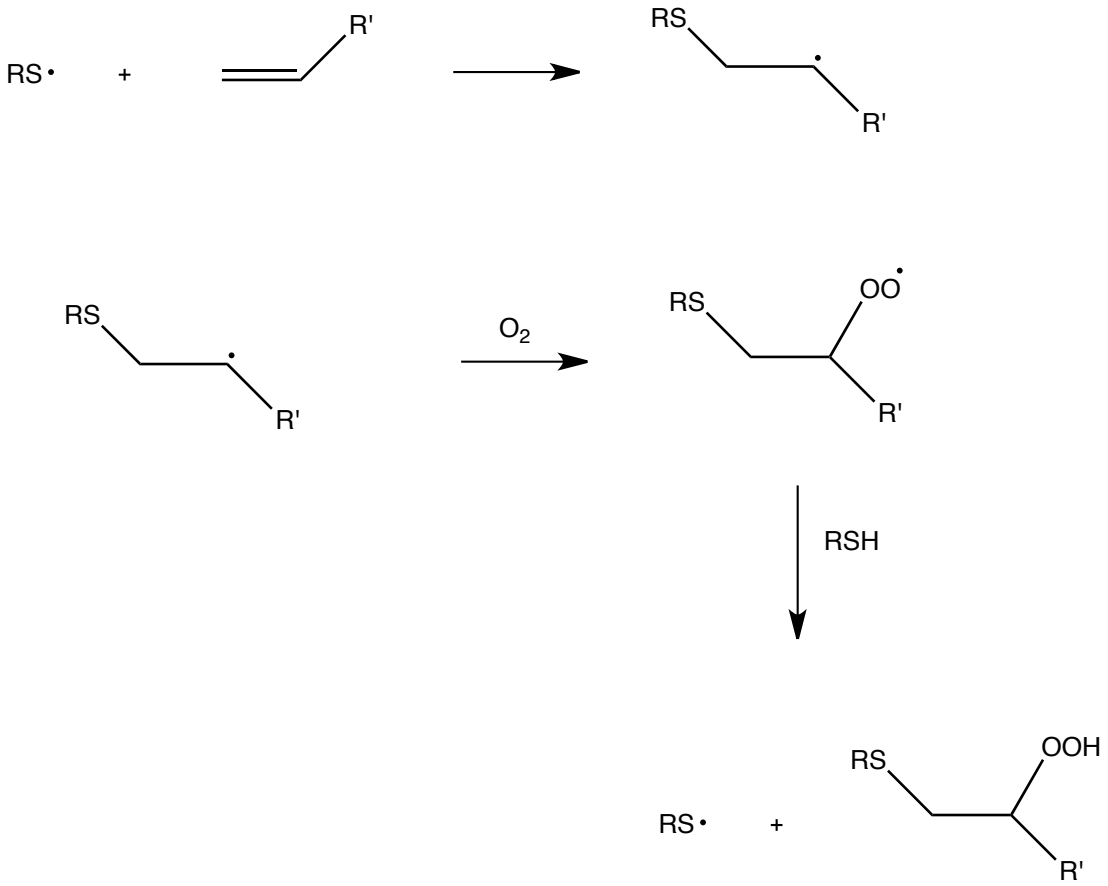

Scheme 4. Oxygen scavenging mechanism for thiol molecule [23]

2.2.2 Initiators

Thiol-ene systems are amenable for different methods of initiation such as thermal, redox or photo initiation [24-27]. Furthermore, these systems are so reactive that, the polymerization can be initiated even without an initiator but with the charge transfer interactions between thiol and ene molecules [23]. Photopolymerization method is mostly utilized for the synthesis of thiol-ene

networks due to the experimental convenience and the opportunity of interrupting the reaction. In the present study photopolymerization technique is applied as well.

Thiol-ene photo polymerization can be initiated by excitation of type 1 photo initiators which undergo alpha-cleavage of an aromatic ketone upon excitation, or type 2 photo initiators that abstracts hydrogen from a hydrogen donor or simply by excitation of thiol monomer that is followed by a lysis of the sulfur-hydrogen bond. [11, 28]. An example of radical formation for a type 1 photo initiator, namely dimethoxyphenyl acetophenone (DMPA) is shown in scheme 5. By the absorption of a photon of light, a benzoyl and a tertiary carbon radical is formed and then the tertiary carbon radical rearranges to give a methyl radical. Both methyl and benzoyl radicals are capable of initiating the thiol-ene reaction.

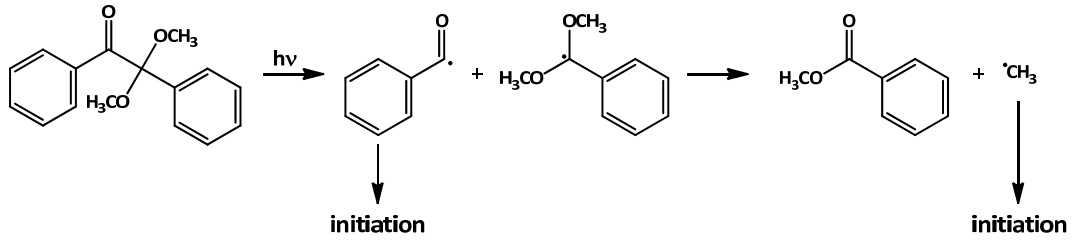

Scheme 5. Radical formation by the cleavage type photoinitiator, namely, DMPA.

On the other hand, the mechanism of radical formation is different for type 2 photoinitiators. An example of disintegration mechanism, namely for camphorquinone is given in scheme 6. Upon irradiation at the absorption wavelength range (400-500nm), dicarbonyl cromophore group on camphorquinone is excited to its singlet state by an (n,π*) transition and by intersystem crossing it proceeds to the respective triplet state. It is then capable of abstracting a hydrogen atom from the relatively weak SH bond, creating a thiyl radical which can subsequently start the polymerization [29]. The additionally formed hydrogenated camphorquinone radical cannot initiate a polymerization due to its steric hindrance.

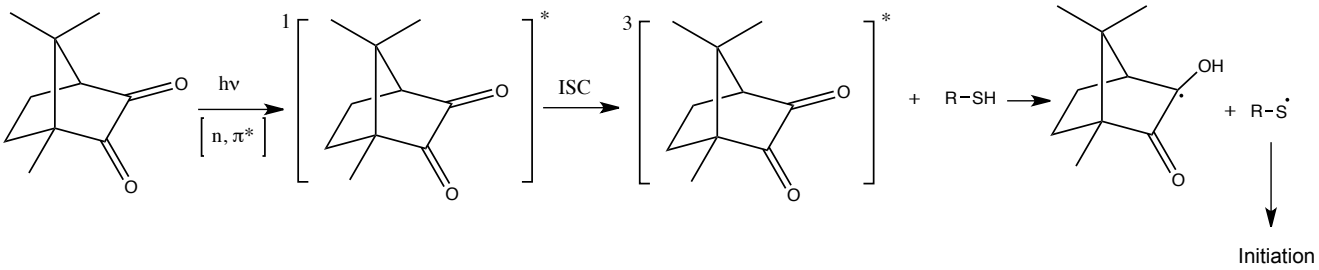

Scheme 6. Formation of thyl radical with camphorquinone photoinitiator

2.2.3 Properties of Thiol-Ene Polymers

Thiol-ene networks are claimed to be more homogenous than those synthesized by free radical chain copolymerization mechanism [12-13]. Dynamic mechanical analysis (DMA) show that during glass transition, networks synthesized via thiol-ene mechanism show narrower *tanδ* peaks than the networks sythesized by free radical crosslinking copolymerization as shown in scheme 7. This means that the chain lengths between crosslink points are more homogenously distributed for thiol-ene networks. The main reason for such behavior is the high conversion of monomers at the gel point due to the step growth character of the thiol-ene mechanism.

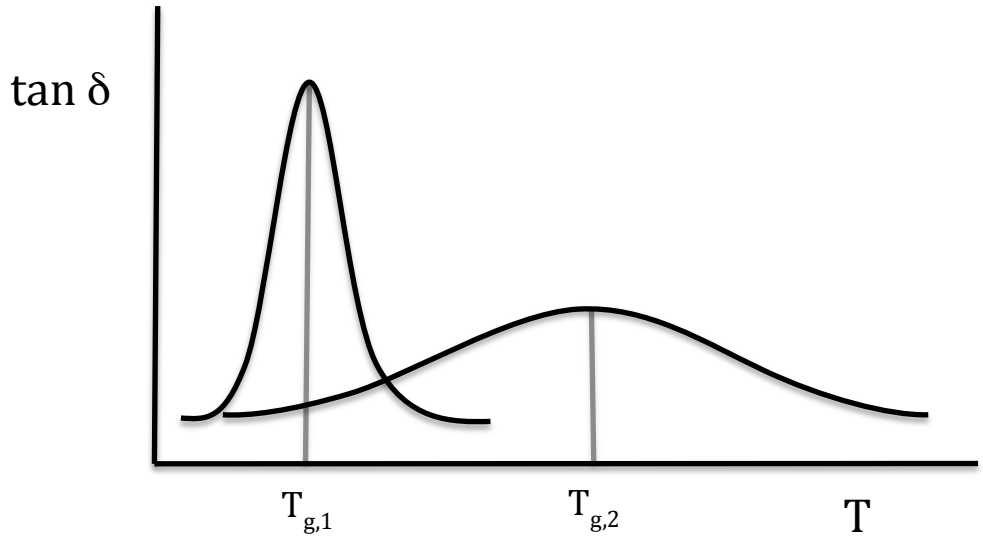

Scheme 7. the loss tangent, tanδ at the glass transition of differently prepared networks plotted versus temperature. Narrow and broad curves belong to the networks synthesized via thiol-ene and free radical crosslinking copolymerization respectively. [12-13]

In order to quantify this behavior, the Carothers equation has to be modified [15] due to the additional functional groups on monomers that lead to the network formation. For this purpose, a functionality factor, f_{av}, which is equal to the average number of functional groups per reactive molecule is calculated with equation 3,

$$f_{av} = \frac{n_R \bullet f}{n} \tag{3}$$

where n_R, f and n are the mole of the reactant, functionality of the reactant and the total number of moles in the reaction mixture respectively. After insertion of the equation 3 into the Carothers equation, one obtains

$$DP = \frac{2}{2 - pf_{av}} \tag{4}$$

The critical conversion, p_{crit}, that leads to a theoretically infinite degree of polymerization becomes,

$$p_{crit} = \frac{2}{f_{av}} \tag{5}$$

So, for a reaction between a tetrafunctional thiol and a difunctional ene the average functionality can be calculated as 2.667 and the critical conversion that leads to an infinite network formation becomes 0.75.

3 METHODS

As mentioned in section 2.2.3, thiol-ene networks are considered as uniform structures because their DMA thermograms show narrow glass transition regions. This behavior is associated with the polydispersity of the network chains. The aim of this study is to use more direct methods such as dynamic light scattering and rheology to monitor the microstructure of the thiol-ene networks.

3.1 Dynamic Light Scattering

Dynamic light scattering (DLS) is one of the most powerful tools employed to characterize the structure and dynamics of polymer solutions with micelles or aggregates [30,31], proteins [32,33], bulk copolymers [34] and polymer networks [35-41]. A schematic representation of a DLS measurement setup is shown in scheme 8. When a monochromatic, coherent beam of light passes through a polymer solution or gel medium it is scattered in all directions. A photon detector positioned at a certain angle collects the photons scattered in that direction and sends the data to the correlator.

The scattered light intensity, $I(q,t)$, measured over time shows a noisy pattern due to the brownian motions of the species in the observed sample, which seems meaningless at first sight. However treatment of this noisy pattern with equation 6 by a correlator gives a similar decaying autocorrelation function such as shown in Figure 1 [42]. Angular brackets indicate a time averaged quantity [43]. Hence the autocorrelation function calculated is called the time averaged intensity correlation function. q is the amplitude of the scattering vector given by the equation 7, where θ is the scattering angle, n is the refractive index of the medium and λ_0 is the wavelength of the incident light in vacuum.

$$g^{(2)}(q,\tau) = \frac{\langle I(q,t) \cdot I(q,t+\tau) \rangle_T}{\langle I(q,t) \rangle_T^2} \quad (6)$$

$$q = \frac{4\pi n}{\lambda_0} \cdot \sin\left(\frac{\theta}{2}\right) \quad (7)$$

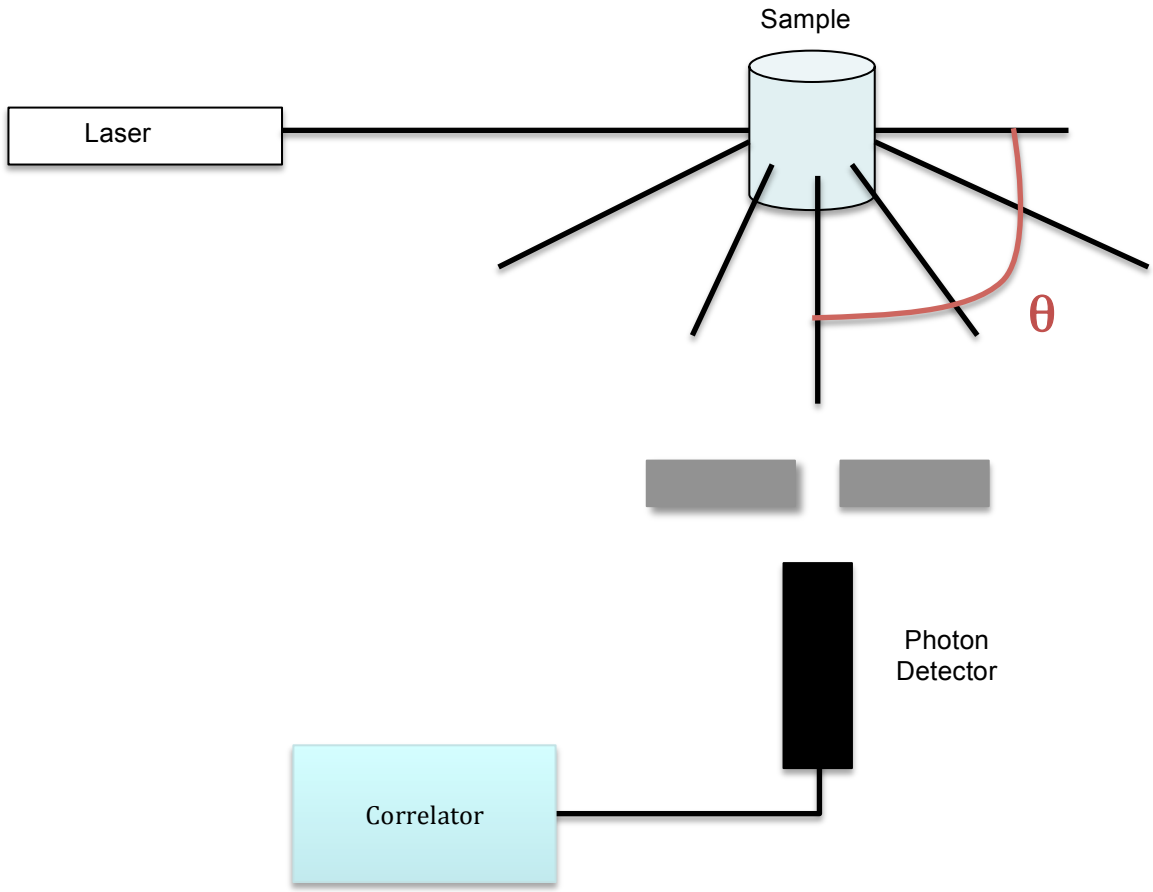

Scheme 8. A simple drawing of DLS instrument

The autocorrelation function, which is often a single exponential decaying function for dilute solutions, contains valuable information about the dynamics of the sample observed. Since instantaneous fluctuations of the intensity of the scattered light depend on thermal motions of the chains, molecules, or

particles one can gather information on the intensity correlation time, $\tau_{(2)}$, of the system from the autocorrelation curve by the use of equation 8 and $\tau_{(2)}$ is connected to the cooperative diffusion coefficient, D, according to equation 9.

$$g^{(2)}\left(q,\tau\right) = \exp\left(-\frac{\tau}{\tau_{(2)}}\right) + 1 \qquad (8)$$

$$\tau_{(2)} = \frac{1}{2Dq^2} \qquad (9)$$

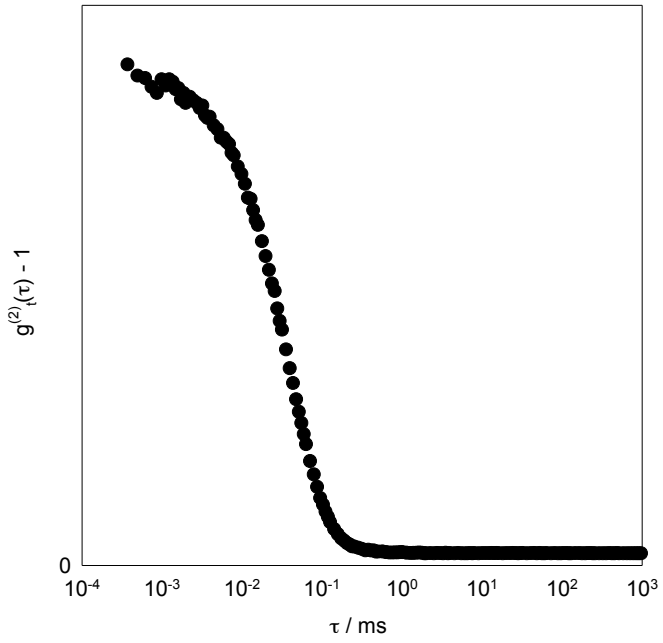

Figure 1. Example of an autocorrelation function obtained from a DLS measurement

Experimental detection of the scattered light is carried out by photon sensitive devices such as photomultiplier tubes. This means that the measured quantity during a dynamic light scattering measurement is the number of photons per unit time arriving at the detector and this quantity is used as a measure of the intensity of the scattered light. However the relevant quantity is basically the electric field. The intensity at a specific time is proportional to the amplitude of the electric field (Eq. 10)

$$I(q,t) \approx \left|E(q,t)\right|^2 \tag{10}$$

The time averaged field correlation function, $g^{(1)}(q,\tau)$, shown in equation 11 is connected to the time averaged intensity correlation function through the Siegert relation (eq. 12).

$$g^{(1)}(q,\tau) = \frac{\left\langle E(q,t) \bullet E^{*}(q,t+\tau)\right\rangle_T}{\left\langle E(q,t)\right\rangle_T^2} \tag{11}$$

$$g^{(2)}(q,\tau) = \left|g^{(1)}(q,\tau)\right|^2 + 1 \tag{12}$$

where E is the amplitude of the field and E* is the conjugate field amplitude.
The Siegert relation applies only to the scattering processes in which the scattered field is a zero mean complex Gaussian variable and the sample is assumed to show a full relaxation during a DLS experiment. However this is not the case for a polymer gel [35,44,45]. During gelation an infinite network is formed with some frozen-in structures and the polymer chains that form the network are confined in this limited space. The scattering obtained from a polymer gel is the combination of these frozen-in structures and freely moving segments of the chains consisting the network. Thus, the time averaged scattering intensities and the amplitude of the electric field can be expressed as

$$\left\langle I\right\rangle_T = \left\langle I\right\rangle_F + I_C \tag{13}$$

$$E(t) = E_F(t) + E_C \tag{14}$$

Where $\langle I \rangle_F$ and I_C, are the light intensities and $E_F(t)$ and E_C are the fields originating from the dynamic and static components in the observed system. respectively.

The relative magnitudes of static and dynamic contributions to the total scattering intensity, which originate from the frozen-in structures and freely moving segments inside the network respectively, are important measures for the inhomogeneity of the network and the mobility of the chains forming it. The so-called nonergodic approach developed by Pusey and van Megen [35] has been proved to be a useful method to separate the portions of scattering intensity from static and dynamic contributions in the network and will be utilized in the context of this dissertation.

3.1.1 Nonergodic Method

For a given fluid-like medium such as colloidal particles in suspension or polymer solutions, a single observation gives a representative information on an observed property as its ensemble average. This is because the system can cover enough possible configurations in the course of a single experiment to represent an ensemble average, which means that the time average magnitude of the property is equal to the ensemble average ($\langle I \rangle_T = I_E$). In other words, the system is ergodic. However the situation for a crosslinked polymer network is not the same. Since the system is connected with physical or chemical crosslinks, the movements of the chains are hindered. Hence, during a single experiment performed on a single sample point the observed part of the whole system cannot cover all the possible configurations to represent an ensemble average through the sample. Then the sample is called nonergodic.

As indicated in the above, the Siegert relation is valid only for ergodic media, and since not all spatial conformations can be assumed to be covered, it does not apply for solid-like systems, like polymer gels. To obtain a self-consistent result over an entire sample, it is necessary to conduct ensemble averaging

over many different sample positions. This can be done by stepwise rotation of the cell or measurements done in many sample points. Generally 100-150 sample positions are considered statistically sufficient. When that condition is assured, one can state the fluctuating field as :

$$\left\langle E_F(q,0)E_F^*(q,\tau)\right\rangle_T = \left\langle E_F(q,0)E_F^*(q,\tau)\right\rangle_E \qquad (15)$$

the right hand side of the equation can be related to the normalized time correlation function as

$$\left\langle E_F(q,0)E_F^*(q,\tau)\right\rangle_E = \left\langle I(q)\right\rangle_E\left[f(q,\tau)-f(q,\infty)\right] \qquad (16)$$

where, $f(q,\tau)$ is the normalized intermediate ensemble averaged scattering function.

At the zero time limit, equation 16 reduces to

$$\left\langle I_F(q)\right\rangle_T = \left\langle I(q)\right\rangle_E\left[1-f(q,\infty)\right] \qquad (17)$$

and, with the necessary rearrangement, the normalized intermediate scattering function for the nonergodic approach becomes,

$$f(q,\tau) = 1+\frac{\left\langle I\right\rangle_{T,p}}{\left\langle I\right\rangle_E}\left[\sqrt{\left(\left(g^{(2)}(q,\tau)-1\right)-\sigma_p^2+1\right)}-1\right] \qquad (18)$$

Where σ^2 defines the intercept of the intensity correlation function.

Figure 2 shows an example of intensity correlation function transformed into the normalized intermediate ensemble averaged scattering function. As can be seen from the figure, resultant curve starts from 1 and relaxes to an offset value. As this curve is fit to the exponential function given by the equation 19, the offset value, $f(q,\infty)$, would give the relative fraction of the scattering originated by the frozen-in parts of the network and the amplitude, *A*, would

give the relative portion of the scattering originated from the dynamic or fluctuating parts in the network.

$$f(q,\tau) = f(q,\infty) + A \cdot \exp\left(-\frac{\tau}{\tau_{(1)}}\right) \qquad (19)$$

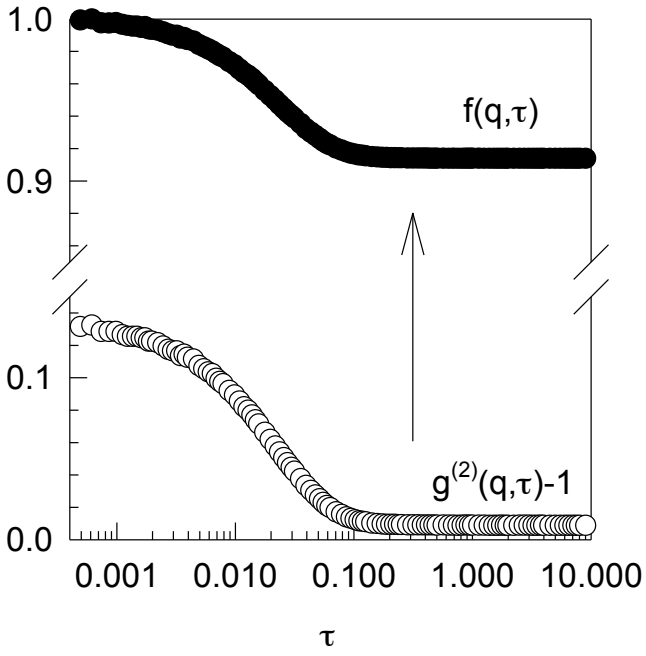

Figure 2. An example of intensity correlation function and normalized intermediate ensemble average scattering function calculated from the same measurement, shown with open and filled symbols respectively.

3.2 Mechanical Characterization[47-50]

Since gels are three dimensional polymer networks, they tend to resist to an applied force. This behavior is directly related to the microstructure of the material. Therefore mechanical characterization is one of the most important methods to gain insight into polymer gels. In the context of this thesis the increase of the shear modulus during gelation, the final shear modulus attained after completion of gelation and the maximum degree of swelling of the gels synthesized are utilized as mechanical characterization methods. So far the theory of viscoelasticity and rubber elasticity are the best fitting

approaches to understand the mechanical behavior of polymer networks [47,48].

3.2.1.Viscoelasticity[47]

Being an intermediate structure between pure solid (elastic) and pure liquid (viscous), a polymer gel shows the combination of both viscous and elastic properties. This means when a shear force is applied as in scheme 9, it reflects both the viscous and the elastic properties of the material [47].

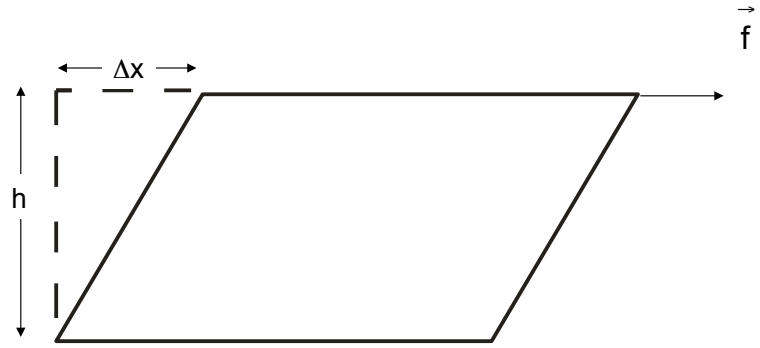

Scheme 9 Shematic illustration of deformation under simple shear.

The shear stress, σ, is defined as the ratio of the applied force, *f*, and the cross-sectional area of the surfaces *A*, which is also the area of any plane perpendicular to the y direction within the material being sheared :

$$\sigma \equiv \frac{f}{A} \qquad (20)$$

The shear strain, γ, is defined as the displacement of the top plate, Δx, relative to the height of the sample *h*:

$$\gamma \equiv \frac{\Delta x}{h} \qquad (21)$$

In case of the observed material being a purely elastic, the ratio of the shear stress and shear strain is constant and gives the shear modulus, *G*:

$$G \equiv \frac{\sigma}{\gamma} \tag{22}$$

On the other hand if the material between the surfaces is a simple liquid, the stress is zero for a constant strain, thus the term shear rate, $\dot{\gamma}$, is introduced instead:

$$\dot{\gamma} \equiv \frac{d\gamma}{dt} \tag{23}$$

For a simple fluid, the shear stress is linearly proportional to the shear rate, which defines the shear viscosity, η :

$$\eta \equiv \frac{\sigma}{\dot{\gamma}} \tag{24}$$

Oscillatory measurements are widely employed in order to characterize the viscoelastic properties of the materials due to both practical and strategical advantages. During an oscillatory shear measurement a sinusoidal strain with angular frequency, ω, is applied to the sample in simple shear :

$$\gamma(t) = \gamma_0 \sin(\omega t) \tag{25}$$

The principal advantage of this technique is the opportunity of observing material properties in different time scales by simply changing the angular frequency. If the material studied is an ideally elastic solid, the stress is related to the strain according to Hooke's law:

$$\sigma(t) = G \cdot \gamma(t) = G \cdot \gamma_0 \sin(\omega t) \tag{26}$$

However if the material being studied is a Newtonian liquid, the stress in the liquid will be related to the shear rate through Newton's law :

$$\sigma(t) = \eta\left(\frac{d\gamma(t)}{dt}\right) = \eta\gamma_0\omega\sin\left(\omega t + \frac{\pi}{2}\right) \qquad (27)$$

The linear response of a viscoelastic material always has stress oscillate at the same frequency as the applied strain but the stress leads the strain by a phase angle, δ, δ being between π and $\pi/2$.

$$\sigma\left(t\right) = \sigma_0\sin\left(\omega t + \delta\right) \qquad (28)$$

Solids which obey Hooke's law have $\delta = 0$ at all frequencies and liquids that obey Newton's law have $\delta = \pi/2$ at all frequencies. Since in the limit of linear viscoelasticity the stress is always a sinusoidal function with the same frequency as the strain, it can be separated into two orthogonal functions which oscillate with the same frequency, one in-phase with the strain and the other out-of-phase with strain by $\pi/2$:

$$\sigma\left(t\right) = \gamma_0\left[G'\left(\omega\right)\sin\left(\omega t\right) + G''\left(\omega\right)\cos\left(\omega t\right)\right] \qquad (29)$$

This equation defines $G'(\omega)$ as the storage (or elastic) modulus and $G''(\omega)$ as the loss (or viscous) modulus :

$$G' = \frac{\sigma_0}{\gamma_0}\cos\left(\delta\right) \qquad (30)$$

$$G'' = \frac{\sigma_0}{\gamma_0}\sin(\delta) \qquad (31)$$

Then the tangent of the phase angle, the loss tangent, is the ratio of loss and storage moduli :

$$\tan(\delta) = \frac{G''}{G'} \qquad (32)$$

The storage and loss moduli are the real and imaginary parts of the complex modulus *G*(ω)* :

$$G^*(\omega) = G'(\omega) + iG''(\omega) \qquad (33)$$

3.2.1 Theory of Rubber-Like Elasticity [48-51]

Rubbers are lightly crosslinked polymeric networks with rather large free volume that allows them to respond to external stress with a rapid rearrangement of the polymer segments [52]. In their swollen states most polymer gels satisfy these criteria for a rubber [53]. Since the theory of rubber elasticity deals with the time independent chain orientation and structure, it takes into account the storage modulus only.

The theory of rubber elasticity assumes that the network chains forming the structure have an ideal Gaussian distribution of the end-to-end distances [54], and has a theoretical crosslink density, ν_{th} , given by the ratio of molar crosslinker concentration to the crosslinker functionality, *f*, as in equation 34 [55]:

$$\upsilon_{th} = \frac{2[XL]}{f} \qquad (34)$$

Two basic network models have been developed in order to describe the elastic behavior of polymer networks [49,55], namely the affine and the

phantom network models. They both assume that the polymer chains forming the network are monodisperse and have a perfect network structure.

3.2.1.1 Affine Network Model [49]

In the affine network model, it is assumed that the relative deformation of each network strand is the same as the macroscopic relative deformation imposed on the whole network and the effect of entanglements is omitted. In this case, the Boltzmann equation can be used to compare the entropy of the network chains before and after deformation

$$S = k_B \ln(W) \tag{35}$$

Here, k_B is the Boltzmann constant and W is the number of chain conformations that can be obtained from the distribution of end-to-end vectors.
If the W value is approximated as a Gaussian function, then the entropy change upon deformation can be given as [56]

$$\Delta S = -\frac{nk_B}{2}(\lambda_x^2 + \lambda_y^2 + \lambda_z^2 - 3) \tag{36}$$

where λ_x, λ_y and λ_z are the relative deformations in x-, y-, and z-directions,

$$L_x = \lambda_x L_{x0} \qquad L_y = \lambda_y L_{y0} \qquad L_z = \lambda_z L_{z0} \tag{37}$$

and, n is the number of elastically effective network strands.
For further simplicity uniaxial deformation is considered only in x-direction and the entropy change is calculated for a constant volume as

$$\Delta S = -\frac{nk_B}{2}(\lambda^2 + \frac{2}{\lambda} - 3) \tag{38}$$

Then the change of free energy, ΔG, can be expressed as

$$\Delta G = -T\Delta S = \frac{nk_B T}{2}\left(\lambda^2 + \frac{2}{\lambda} - 3\right) \qquad (39)$$

As the force required to deform a network is the derivative of the free energy, *G*, with respect to the length along the *x* axis of deformation and as the definition of the stress, σ, is the ratio of force and cross-sectional area, σ becomes

$$\sigma = \frac{nk_B T}{V}(\lambda - \frac{1}{\lambda^2}) \qquad (40)$$

The coefficient that relates the stress and deformation is known as the shear modulus,*G*,

$$G = \frac{nk_B T}{V} = \nu k_B T = \frac{\rho RT}{M_C} \qquad (41)$$

with ν number of network strands per unit volume, M_c the average molecular weight of the strands between crosslink points, ρ the network density (mass per unit volume) and *R* the gas constant.

3.2.1.2 Phantom Network Model [49]

The main assumption in the phantom network model differing from the affine network model is that the junction points inside the network can move freely and chains can pass through each other which also excludes the influence of any entanglements. The crosslink junctions are not fixed in a coordinate system as assumed in the affine network model and can fluctuate about their

average positions. This leads to a drop in their free energy by reducing the cumulative stretching of the network strands. Therefore a structure factor to correct the fluctuation of the f-functional crosslinks is introduced:

$$G = \nu k_B T \frac{f-2}{f} = \frac{\rho RT}{M_C}\left(1-\frac{2}{f}\right) \qquad (42)$$

where *f* is the functionality of a cross-link in the network.

3.3 Swelling [57,58]

One of the most distinct features of polymeric gels is their ability to swell. Since crosslinked polymer networks cannot dissolve in a solvent, they rather swell. A swollen polymer network is actually in an equilibrium state governed by the elastic force that holds the chains together and the osmotic pressure arised from the mixing entropy of the solvent and the network polymer chains. Free energy of swelling, ΔG_{sw}, can be expressed as the combination of free energy of mixing (ΔG_{mix}) and elasticity (ΔG_{El}) :

$$\Delta G_{Sw} = \Delta G_{mix} + \Delta G_{El} \qquad (43)$$

Free energy of mixing for polymer solutions is given by Flory-Huggins relation (eq. 44) [59,60] and energy change with deformation of the network is given in equation 39.

$$\Delta G_{mix} = kT\left(n_1 \ln \upsilon_1 + n_2 \ln \upsilon_2 + n_1 \chi_{12} \upsilon_2\right) \qquad (44)$$

Where n_1, n_2, ν_1, ν_2 and χ_{12} are number of solvent and polymer molecules, volume fraction of solvent and polymer molecules and interaction parameter between polymer and solvent molecules respectively.

With proper rearrangements, free energy change during swelling process is calculated according to the equations 39, 43 and 44 which is known as Flory-Rehner relation:

$$\Delta G_{sw} = RT\left[\ln\left(1-\upsilon_2\right)+\upsilon_2+\chi_{12}\upsilon_2^2+V_1\upsilon\left(\upsilon_2^{1/3}-\frac{\upsilon_2}{2}\right)\right] \qquad (45)$$

Polymeric gels are mostly synthesized in solution by copolymerization of an appropriate monomer and a crosslinking agent or by intermolecular reaction of dissolved polymers that have multiple active sites. Thus, right after the synthesis, a polymer gel is already in a particular swollen state because, as the reaction carried on, the network chains come to an unperturbed conformation driven by just the reaction kinetics and the mobility of the reactants. Hence right after the synthesis state is an important reference point for comparison with the equilibrium swollen state. Equation 42 gives the relative swelling ratio, q_r, as:

$$q_r = \frac{m_{sw}}{m_{ras}} \qquad (46)$$

m_{sw} and m_{ras} are the masses of the gels in equilibrium swollen and right after synthesis states respectively.

The absolute swelling ratio is given by a gels swelling capacity relative to its dried state,

$$q_w = \frac{m_{sw}}{m_{dry}} \qquad (47)$$

4 EXPERIMENTAL

4.1 Chemicals

Pentaerithritol tetrakis(3-mercaptopropionate) (PETMP), and triethyleneglycol divinylether (TEGDVE) are used as tetrafunctional crosslinker and monomer respectively, camphorquinone is used as the photoinitiator and 1,1,2-trichloroethane is used as the solvent. Chemical structures of the monomers, initiator and the solvent are given in scheme 9. Detailed information about the chemicals used are given in Appendix 1.

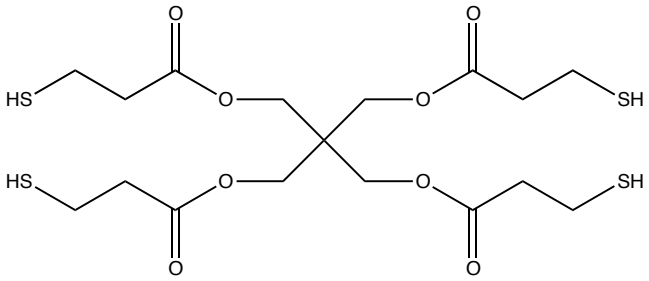

Pentaerithritol trimercaptopropionate

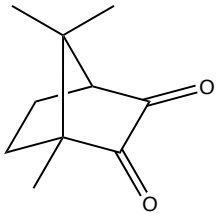

Camphorquinone

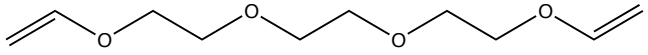

Triethyleneglycol divinylether

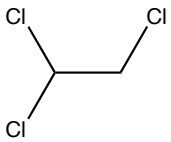

1,1,2-trichlorethane

Scheme 9. Chemical structures of the tetra-functional crosslinker, monomer, photoinitiator and the solvent used in gelation reactions.

4.2 UV/VIS Measurements

Jasco V-550 UV/VIS spectrophotometer was used to make sure that the absorption bands of monomers and the photoinitiator do not overlap. UV absorption graphs for a reaction mixture of 10% (w/v) monomer concentration and camphorquinone solution are shown in Figure 3. As shown PETMP-TEGDVE mixture have a strong absorption between 350-370 nm. On the other hand, absorption band of the initiator at higher wavelengths, i.e. 400 – 500 nm does not interfere with that of monomers. Thus in order to obtain a controllable light intensity through the sample a photoinitiator with a different absorption wavelength, i.e., 465 nm, was used. As a calibration curve was generated for camphorquinone, the molar absorption coefficient is found to be 43.21 $L.mol^{-1}.cm^{-1}$ and 90 % of transmission through the DLS cuvettes during illumination was obtained at 1.21 mM concentration. Smaller amounts of initiator down to 0.3 mM is also used for the synthesis of thiol-ene organogels. However, no change in scattering intensities and network density values are observed. Hence, the value 1.21 mM is fixed as the initiator content.

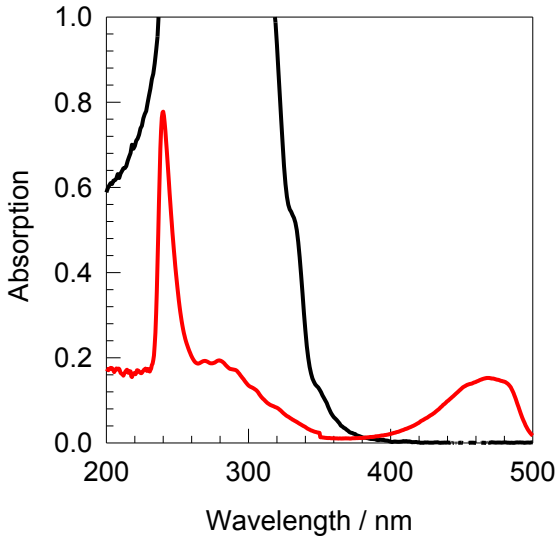

Figure 3. Absorption spectra of 10% monomer mixture composed of PETMP-TEGDVE and 3.6 mM camphorquinone shown with black and red curves respectively.

4.3 Synthesis of Thiol-Ene Organogels

The calculated amount of thiol crosslinker PETMP, solvent, ene monomer TEGDVE and photoinitiator stock solution were mixed in that order to reach the calculated volume and the accurate concentration. Since the sampling of reactants for the synthesis were practiced gravimetrically, all the concentrations are given in weight percent unless stated otherwise. The concentration of the photoinitiator was kept constant at 1.21 mM as mentioned in previous section. Amounts of chemicals used in synthesis are given in Appendix 2.

After mixing the components in a flask, the reaction was conducted in three different media, for DLS measurements in a DLS cuvette with the inner diameter of 0.875 ± 0.025 cm, for swelling measurements in a glass tube with an inner diameter of 0.23 cm and on the rheometer plate. The samples in DLS cuvette and glass tubes were illuminated for 5 hours and for rheological measurements illumination time was limited to that of obtaining a steady moduli plateau during the measurement. Samples for near-infrared (NIR) measurements were filtered in a quartz cuvette with 1 cm width. An LED blue light set-up that has a peak-intensity wavelength of 465 nm was used for illumination.

4.4 Dynamic Light Scattering Measurements

DLS measurements were performed with an ALV/CGS-3 compact goniometer (ALV GmbH) equipped with a helium-neon laser with a wavelength of 632.8 nm, ALV/LSE-5003 correlator, a cuvette rotation/translation unit for measuring nonergodic samples and fiber optical three mode detection optics combined with an ALV/HIGH QE avalanche photodiode detector. All the measurements were performed at 25°C and at scattering angles between 50°-130°. However, preliminary results showed that the samples measured did not show any angle dependencies, thus the majority of the measurements were performed at θ=90°. After placing the cuvettes into the toluene bath inside the DLS

instrument, the samples were allowed to thermally equilibriate for approximately 10 minutes before the measurements start.

Three sets of measurements were carried out for the application of nonergodic approach and to reveal the position dependency of the time average scattering intensity of the gel samples. For each sample a single measurement was performed in order to obtain an ensemble average scattering intensity, I_E, value while the cuvette was constantly rotating. Then another 15 measurements were carried out at different sample positions, performing 1200 seconds for each in order to obtain a smooth autocorrelation curve for application of nonergodic approach and finally 100 measurements at different sample positions for 30 seconds to show the position dependency of the time average scattering intensity. On the other hand, for gelation study, just ten measurements are performed at different positions. Illumination was turned off during all measurements.

4.4.1 The Coherence Factor β

The intercept of the intensity correlation function, σ^2, is affected by the character of the sample and the detection optics. The theoretical value of σ^2 for a homodyne sample is 1. However this value cannot be observed for the instrument employed in current study, since a three-mode fibre optic detection unit is utilized within and the term, coherence factor (β) is introduced which is defined as in equation 48 [61]:

$$\beta \leq \frac{1}{\aleph} \qquad (48)$$

Where $\aleph$ is the number of modes.

With increasing number of modes, the average signal intensity is also increases, however the coherence factor, i.e. the amplitude of the dynamic part of the multimode correlation function, decreases correspondingly. If the coherence factor is taken into account for the mentioned instrumental setup

that is utilized for the current study, equation 18 should be rewritten as in equation 49:

$$f(q,\tau) = 1 + \frac{\langle I \rangle_T}{\langle I \rangle_E} \left[\sqrt{\left(\frac{\left(g^{(2)}(q,\tau) - 1 \right) - \sigma^2}{\beta} + 1 \right)} - 1 \right] \qquad (49)$$

In order to ensure that the correct coherence factor is used for nonergodic approach calculations, scattering intensities from dilute polystyrene solutions prepared at different concentrations are plotted against the intercept of intensity correlation function according to equation 50 [62],

$$g^{(2)}(0) - 1 = \left(1 - \frac{I_0}{I} \right)^2 \cdot \beta \qquad (50)$$

where I_0 is the scattering intensity of pure solvent, *I* is the scattering intensity of polymer solution, $g^{(2)}(0) - 1$ is the intercept of intensity correlation function. Molecular weight of polystyrene used for preparation of the polymer solutions was 212,000 g/mol. In order to obtain minimize the concentration errors 5mg/ml of polymer stock solution is prepared and diluted to different concentrations. Slope of the two lines created toluene and 1,1,2-trichlorethane result two different but close β values, i.e., 0.424 and 0.412 respectively. Since 1,1,2-trichlorethane is used as the reaction solvent, 0.412 is taken as the β value.

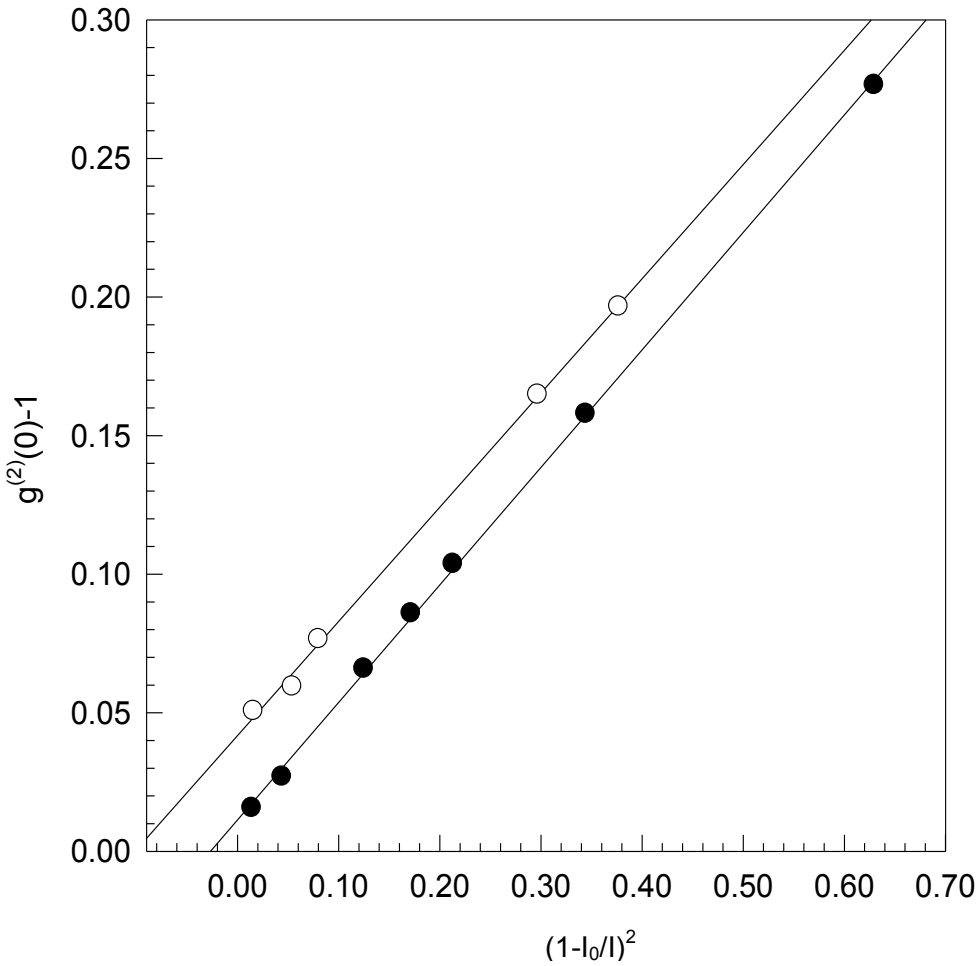

Figure 4. Variation of the intercept of intensity correlation function with the scattering intensity at different linear polystrene concentrations (M_w = 212,000 g/mol). For filled and open symbols toluene and 1,1,2-trichlorethane are used as solvent respectively.

4.5 Rheological Measurements

Rheological measurements were carried out with a Bohlin Gemini 150 rheometer system equipped with a cone-and-plate geometry (40mm diameter and 4° cone angle), a quartz glass bottom plate which lets the blue light pass through without any significant absorption and an LED-illumination system placed underneath as 465 nm light source. A picture of the setup is shown in Figure 5.

After the reaction mixture was prepared, it was placed on the quartz plate and the cone was lowered so that the gap between cone and plate would be 150 μm. Once the full contact of the sample and cone was ensured the illumination was turned on and the reaction allowed to start. Illumination was

Figure 5. Rheometer setup for in situ photocrosslinking.

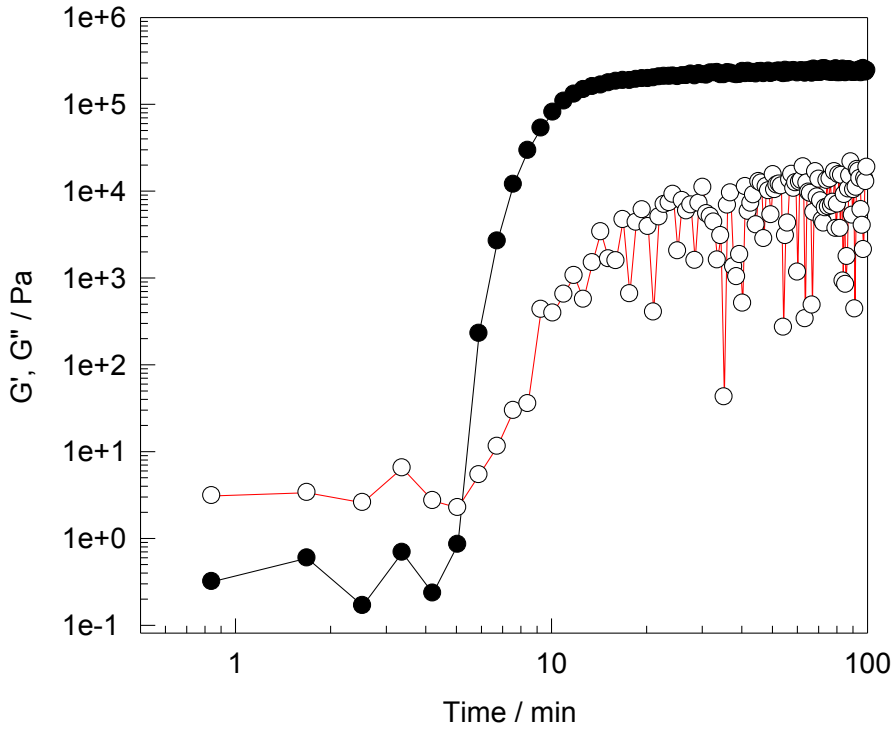

Figure 6. Growth of elastic (G') and viscous (G") moduli during the gelation reaction of 20% (w/v) monomer concentration. Filled and open symbols represent G' and G" respectively

not turned off until the elastic modulus leveled off to a plateau value. An example of rheological measurement is shown in Figure 6.

4.6 Swelling

After 5 hours of illumination, the tubes were broken and the gel samples were immersed into the excess of the solvent after weighting. Swelling of thiol-ene networks were followed gravimetrically and solvent that the gels were swelling in was changed every other day until the swelling equilibrium was reached.

4.7 NIR Measurements

Since vinyl groups have absorption between 1612-1640 nm, near-infrared (NIR) measurements were conducted in order to monitor the conversion of double bonds using a Jasco V-670 NIR spectrophotometer. Figure 7 shows an example of variation in NIR spectra of TEGDVE during a thiol-ene gelation reaction with 20% monomer concentration.

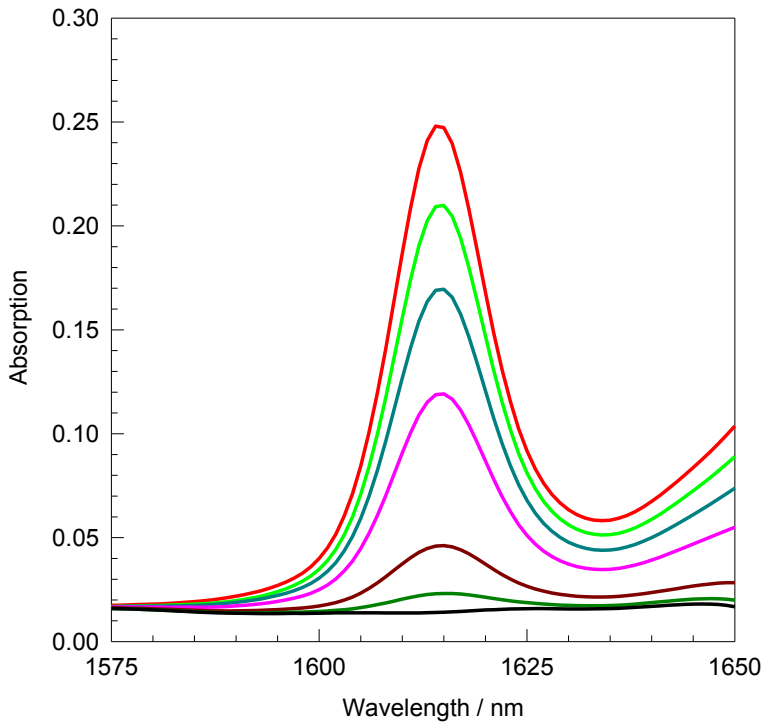

Figure 7. Variation of absorption spectra of TEGDVE during thiol-ene gelation reaction. Measurements were taken at 0, 2, 3, 4, 5, 6, 7 and 10 minutes of reaction time from top to bottom, respectively.

5 RESULTS AND DISCUSSION

A tetra functional thiol, pentaerithritol tetrakis(3-mercaptopropionate) (PETMP), and a difunctional ene, triethyleneglycoldivinylether (TEGDVE) are photochemically crosslinked to form thiol-ene organogels. Investigation of gelation process is carried out by dynamic light scattering (DLS), rheometer and near infra-red spectroscopy (NIR). Dynamic light scattering method is also utilized for revealing inhomogeneity of the resultant gels.

5.1 Gel Formation

DLS measurements are performed at certain reaction times after the illumination of the monomer mixture starts. In order to control the progress of the reaction without illumination, rheological measurements of two thiol-ene organogels at the same monomer concentration are compared. In Figure 8, plot A shows the thiol-ene photopolymerization reaction that is disturbed by turning the illumination off for certain time intervals. Data points obtained without illumination are shown in red circles. On the other hand plot B depicts the measurement carried out with continuous illumination. Both reaction mixtures contain 20% (w/v) monomer concentration. Since the growth of elastic modulus is a direct indicator of the crosslinking reaction taking place, this comparison shows how turning off the illumination affects the reaction and the final crosslink density.

As can be seen from Figure 8, growth of elastic modulus delayed during non-illuminated intervals of the reaction time. For low moduli values about 1 kPa, the reaction does not seem to stop completely but proceeds quite slowly and as the illumination is turned on, the reaction continues again. Also the comparison with the undisturbed reaction in plot B shows that the final modulus obtained in this particular experiment is equivalent to the modulus that is obtained in a continuous reaction carried out with the same monomer concentration. So, Figure 8 implies that we can gather reliable information

from the DLS and near infrared absorption (NIR) measurements conducted during the dark periods of the gelation process to investigate the change of the microstructure of the reaction medium and the conversion of the ene molecules in a thiol-ene crosslinking reaction respectively.

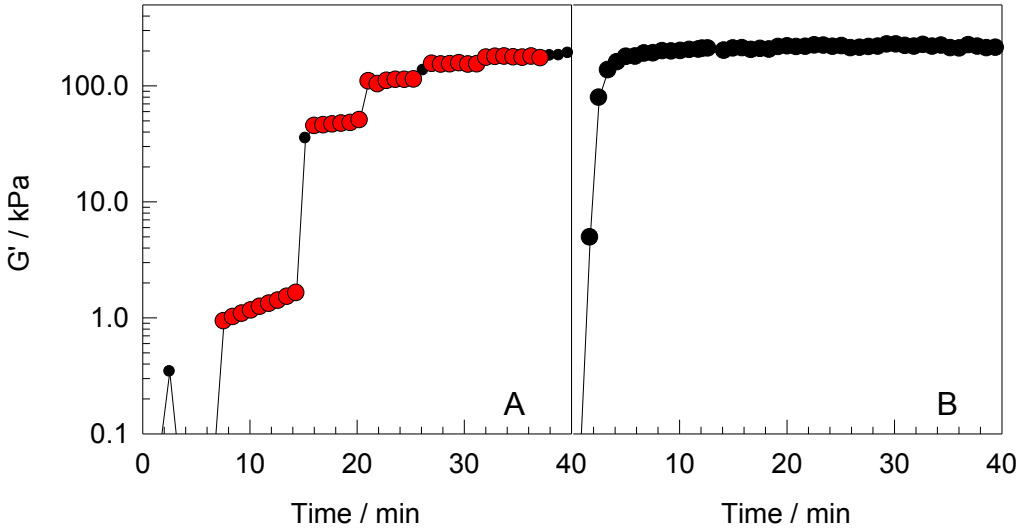

Figure 8. Rheological measurements of 20% (w/v) thiol-ene mixture. Plot A and B show the measurements in which illumination is turned off for certain time intervals and the one that let react without any disturbance, respectively. Data points shown with red circles in plot A show the time intervals that the illumination turned off.

Figure 9 shows the variation of average scattering intensity of the thiol-ene mixture at 20% (w/v) concentration with reaction time at a fixed scattering angle, 90°. During the light scattering measurements no illumination was applied and since the reaction does not continue without light as shown in Figure 8 the microstructure of the sample is assumed to have no major transformations.

According to Figure 9 the scattering intensity starts to increase gradually 3 minutes after the illumination is started and rapidly reaches to a maximum at 10^{th} minute. $\langle I \rangle_E$ starts to decrease and fluctuate after that point due to the merging of clusters which results in the reduction of refractive index fluctuation as well as the dynamic character through the whole structure. The scattering intensity of the light from the final state of thiol-en network is quite low and does not even reach twice the intensity of the sol state. This small

difference between sol and gel scattering suggests that the thiol-ene organogels show a homogenous microstructure. However homogeneity of the studied network may not be the only reason for low scattering intensity. Since the intensity of scattered light from a gel sample increases with the refractive index fluctuations, a small refractive index difference between the gel and the medium, i.e., the solvent, would also result in a low intensity of scattered light. Results of more detailed experiments for a better understanding of the nature of the corresponding networks and related analyses will be given in the next sections of this chapter.

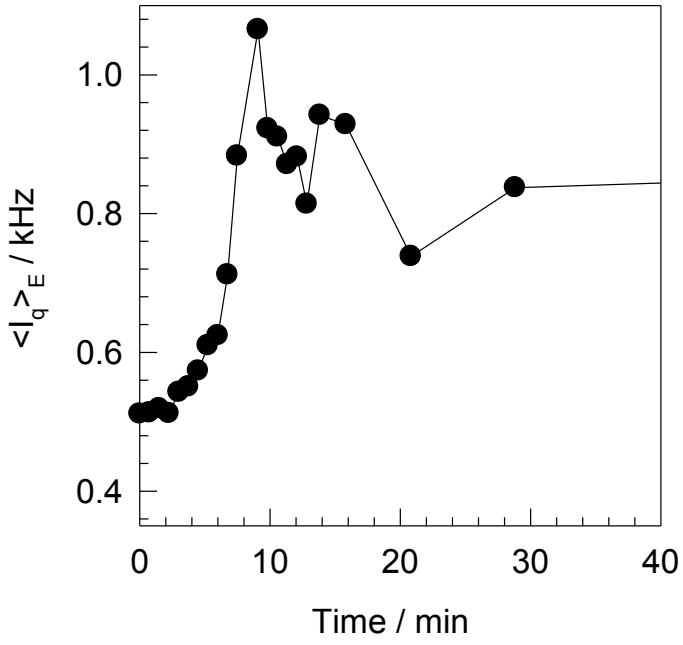

Figure 9. Variation of ensemble average scattering intensity ($<I>_E$) of 20% (w/v) gel with reaction time.

Intensity correlation functions obtained for different reaction times are plotted on double logarithmic scale in Figure 10. In the beginning of the reaction, t=0, there is no obvious relaxation, however with increasing reaction time, a fast relaxation at approximately 10^{-2} ms can be observed, which is first visible at 5.5 minutes. The gel point is observed as the power-law behavior at 6th minute and after that the fast relaxation emerges rapidly, shifting towards slightly longer relaxation times which indicates the merging of the clusters and formation of the network. It should be noted that the correlation functions

obtained at t<6min are somewhat doubtful because the scattering intensity is very low.

DLS measurements conducted at different sample positions at different reaction times are shown in Figure 11. It is clear that the time average scattering intensity starts to fluctuate with sample position approximately 7 minutes after the reaction has started. It is interesting that the strong fluctuations in time average scattering intensity start not at the gel point but after the gelation. This suggests that a relatively uniform three dimensional structure is formed just in the beginning of the gelation and then with increasing time of reaction, i.e. increasing conversion of the monomers, the structure becomes more inhomogeneous.

In order to study this behavior in a systematic way, three sets of gelation reactions are carried out with different monomer concentrations at 10, 20 and 30 % (w/v). Conversion of the difunctional ene molecule is followed by NIR spectrophotometer and gelation point is determined by turning the cuvette upside-down. The results are shown in Figure 12. As can be seen from the figure, gelation for each concentration achieved at different conversions but approximately the same reaction times, between 6-7 minutes. Figure also shows that conversion at the gel point decreases with increasing monomer concentration. This makes sense because the gelation can not occur until the critical overlap concentration is reached which can be obtained with lower conversions at higher monomer concentrations. However even for the 30% concentration, the gel point is achieved at approximately 70% monomer conversion. It should be noted that, the critical conversion observed in NIR measurements are actually in a good agreement with the theoretical value calculated with equation 5.

After the gel point is reached, clusters in the structure become immobile and start to react intramolecularly and this phenomenon give rise to the position dependency of the time average scattering intensity, i.e. the speckle pattern.

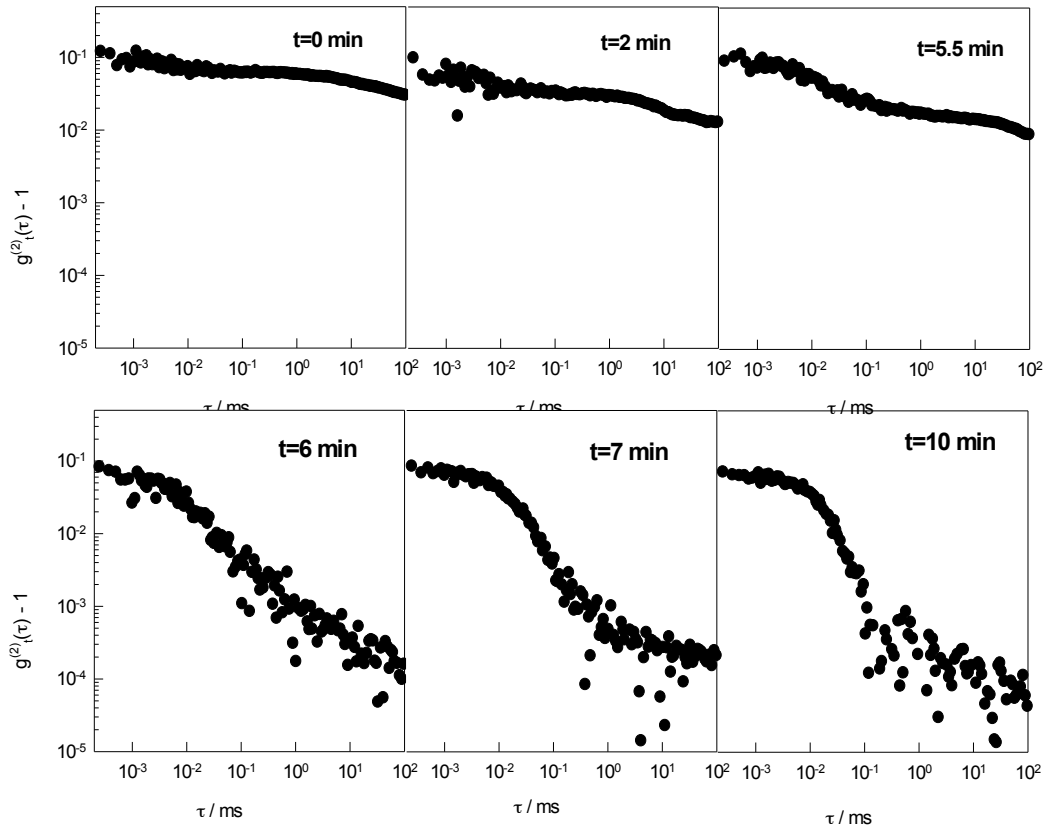

Figure 10. Double-logarithmic plots of the intensity time correlation functions (ICFs) during polymerization of 20% (w/v) thiol-ene organogel.

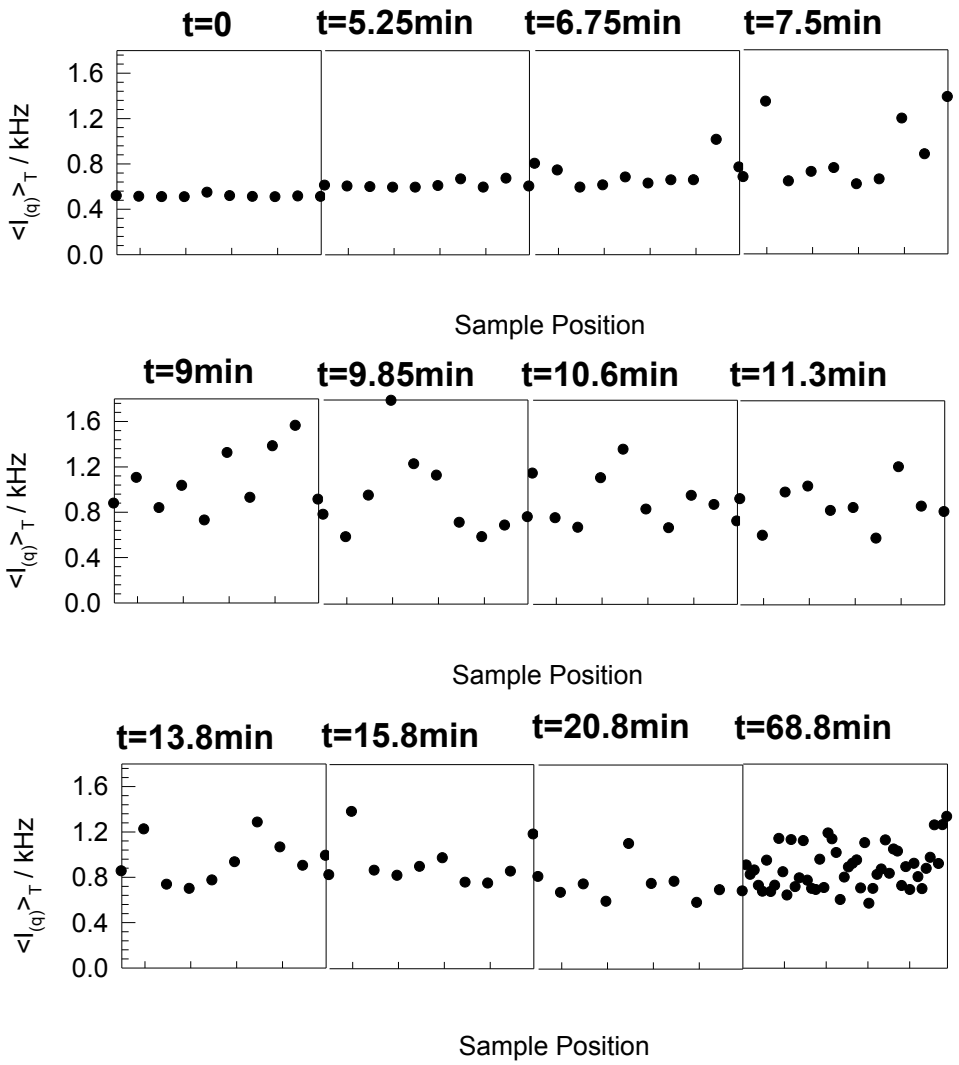

Figure 11. Formation of speckle pattern through the course of the thiol-en gelation reaction at 20% (w/v) monomer concentration.

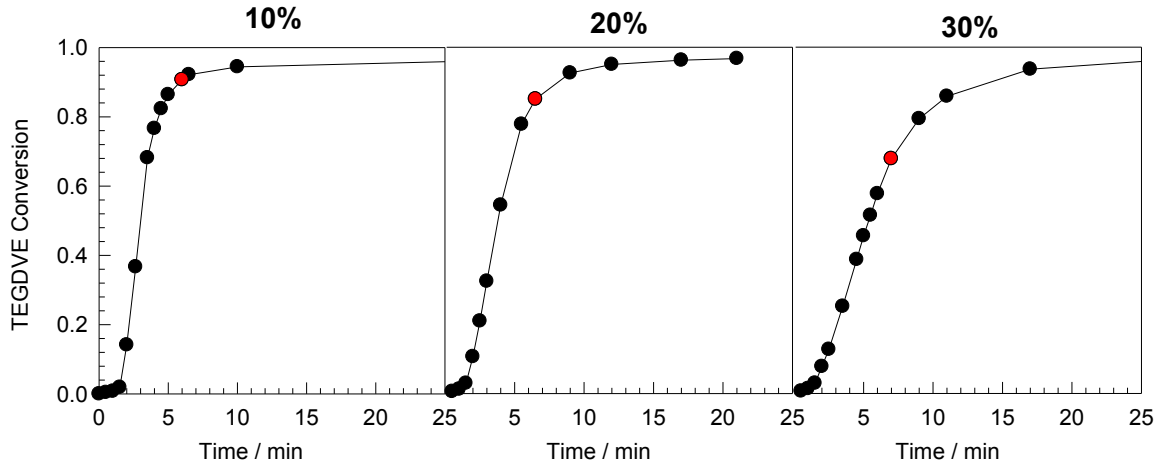

Figure 12. Conversion of TEGDVE over the reaction time with 10, 20 and 30% (w/v) total monomer concentration. Data points shown in red are the reaction times that the gel points were reached.

Growth of elastic moduli during gelation of thiol-ene organogels are investigated by rheological measurements. For this purpose, a mixture of thiol and ene monomers in a specific concentration is simply let react under cone and plate geometry during the illumination. Some examplary measurements carried out with different monomer concentrations are shown in Figure 13. As can be seen from the figure a maximum value is obtained and after that the modulus value is reduced during the measurements for the concentrations below 15%. This behavior is probably due to syneresis [62,63]. This could make sense if the short TEGDVE chains between the PETMP crosslinkers are considered. As the reaction continues the clusters formed in the beginning start to combine, forming a more compact network structure than the volume of the reaction mixture in the beginning of the reaction and to a reduction of the gel volume under the cone. As the syneresis takes place, a decrease is observed in the elastic modulus growth curve. However this behavior is not observed for higher monomer concentrations because the polymer concentration is high enough to fill all the volume in the solvent.

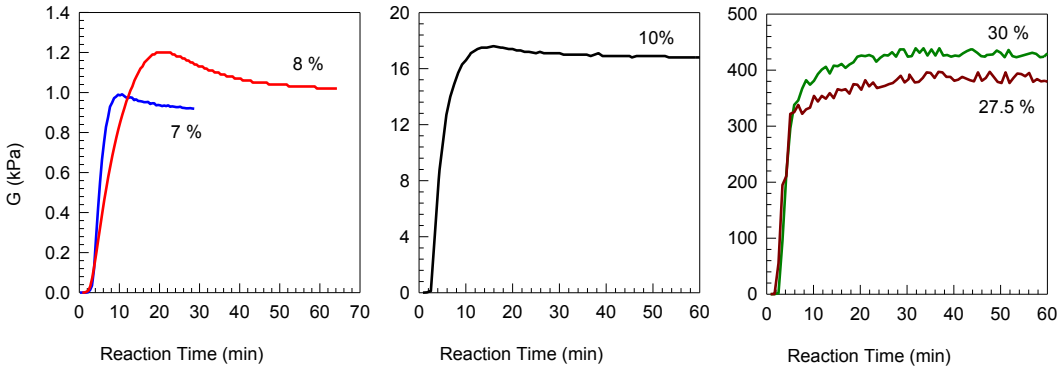

Figure 13. Growth of the Elastic Moduli, G', versus time during the thiol-ene crosslinking reaction at different monomer concentrations.

5.2 Elasticity and Swelling

Figure 14 shows the elastic moduli of the thiol-ene gels synthesized at different concentrations. Note that no gel is formed at monomer concentrations below 7%. As the concentration increases, the elastic moduli of the gels increase almost linearly up to 40% of monomer concentration. Then the increase of the modulus with monomer concentration deviates from linearity. Finally there is not much of difference between modulus values of 80% and the bulk reactions. Leveling off of the elastic modulus may be associated with the hindered mobility of the active chains due to the high modulus value of the gels and the short TEGDVE chains between the crosslink points.

The effective crosslink density calculated from the elastic moduli values are shown in Figure 15. Since elastic moduli of the gels synthesized ranges from a few kPa to MPa, the transition of the gels from phantom to affine network model is unclear. Thus the effective crosslink densities are calculated according to both affine and phantom network models according to the equations 42 and 43. Calculated values from the experimental data are quite below the theoretical line. But still, the effective crosslink density increases linearly up to 40% of monomer concentration and then a plateau region is observed. As can be seen from the plot the calculated values of effective crosslink density do not change much above 50% of monomer concentration.

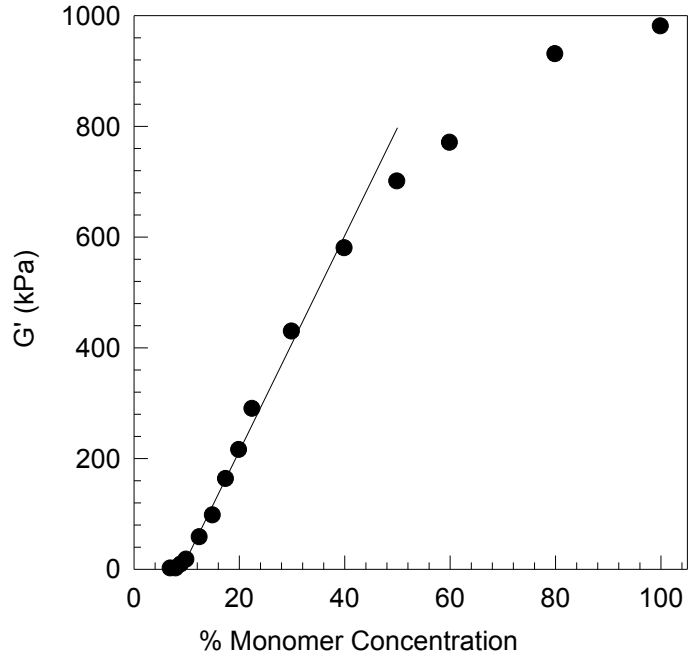

Figure 14. Variation of elastic moduli (G') with % monomer concentration of thiol-ene organogels.

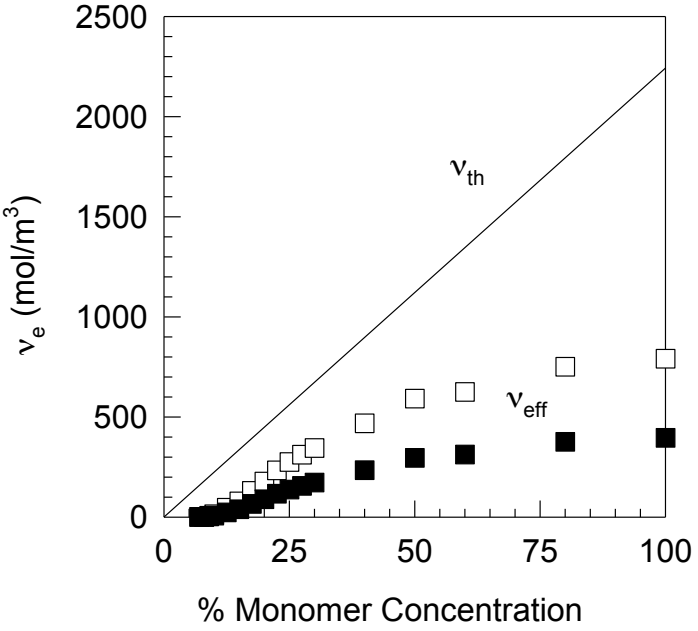

Figure 15. Calculated values of effective crosslink densities and the theoretical crosslink densites of thiol-ene organogels synthesized at different monomer concentrations. Diagonal line, open squares and filled squares show the theoretical crosslink density, effective crosslink density calculated by phantom network model, and effective crosslink density calculated by affine network model, respectively.

The effect of increasing monomer concentration on the crosslinking behavior of the thiol-ene organogels is shown in Figure 16. The crosslinking efficiency is simply calculated by taking the ratio of the theoretical and the effective crosslink density shown in Figure 15. As expected from the previous results and graphs, efficiency of the crosslinking reaction increases up to 40% of monomer concentration and then starts to decrease significantly due to the stiffness of the network and the hindered mobility of the active chains. This would give rise to the intramolecular reactions and cyclizations, which eventually decrease the efficiency of effective crosslinking reactions.

The efficiency of the effective crosslinking reactions increases up to 60% for the phantom network model and 30% for the affine network model. Both values can be considered as high and efficient compared to free radical crosslinking copolymerization reactions.

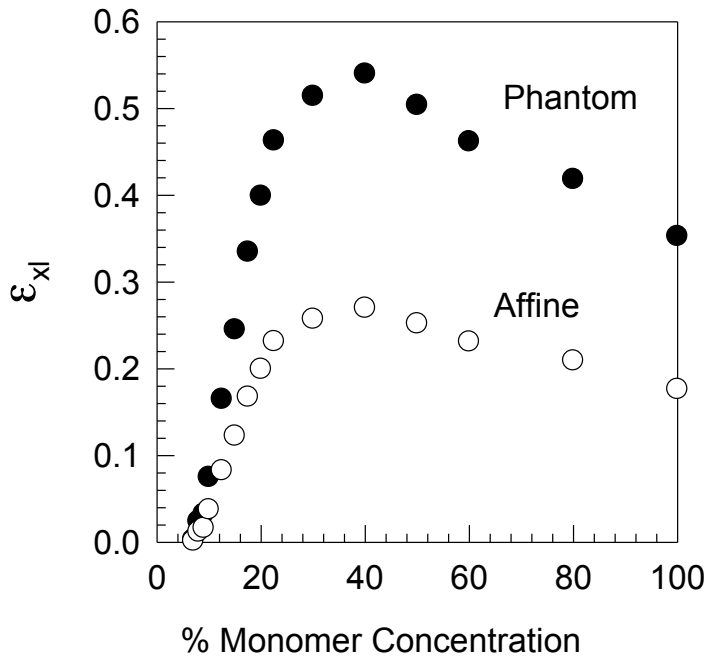

Figure 16. Crosslinker efficiencies of thiol-ene organogels synthesized at different monomer concentrations, calculated by the theoretical and the effective crosslink densities of the networks formed. Open and filled symbols represent the results of the calculations according to affine and phantom network models respectively.

Swelling measurements of the gels are conducted by immersing the gels into an excess amount of solvent and let them swell for at least a week by renewing the solvent every day until the masses of the samples do not

change and stabilize. After swelling the gels are let dry in the oven for at least two weeks and their weight checked every other day until weight loss is completed. Figure 17 shows the absolute swelling ratio (m_{sw}/m_{dry}) of the gels synthesized with different monomer concentrations. Gels synthesized from bulk and 80% monomer concentrations are crumbled during swelling process. The swelling degree of the gels decreases constantly, which is to be expected since the amount of crosslink points increase as the monomer concentration increases. However, the relative swelling ratio shown in Figure 18 exhibits a linear increase with increasing monomer concentration which can be explained with increasing osmotic preassure originated from the increase of polymer concentration inside the gel.

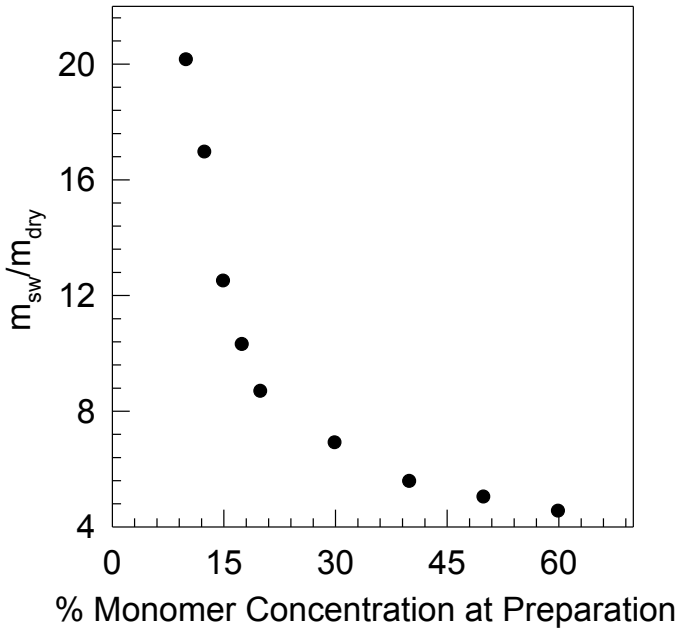

Figure 17. Absolute swelling ratio of thiol-ene gels as a function of monomer concentration at preparation.

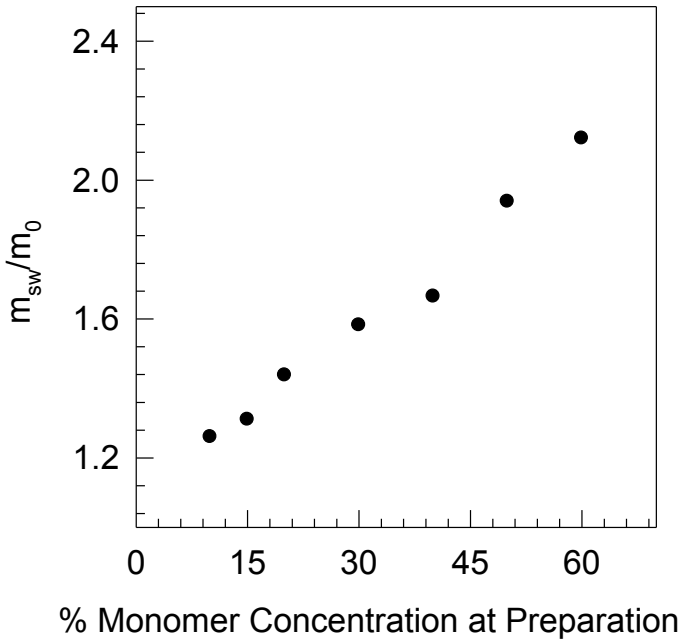

Figure 18. Relative swelling ratio of thiol-ene gels as a function of monomer concentration at preparation.

5.3 Dynamic Light Scattering

Dynamic light scattering measurements are conducted in order to investigate the microstructure and the inhomogeneity of the thiol-ene gels. Measurements are carried out between 8 % and 40 % monomer concentrations and the scattering angle is kept constant at 90° because, as mentioned in experimental section, thiol-ene gels that are synthesized do not show any angle dependency.

Examples of intensity correlation functions (ICF) obtained by a single measurement of the gels are shown in the Figure 19. The initial amplitude of the correlation function decreases which indicates the increase of nonergodicity as the networks get more concentrated. Note that the ICF curves for 30 and 40 % monomer concentration overlap and look quite similar.

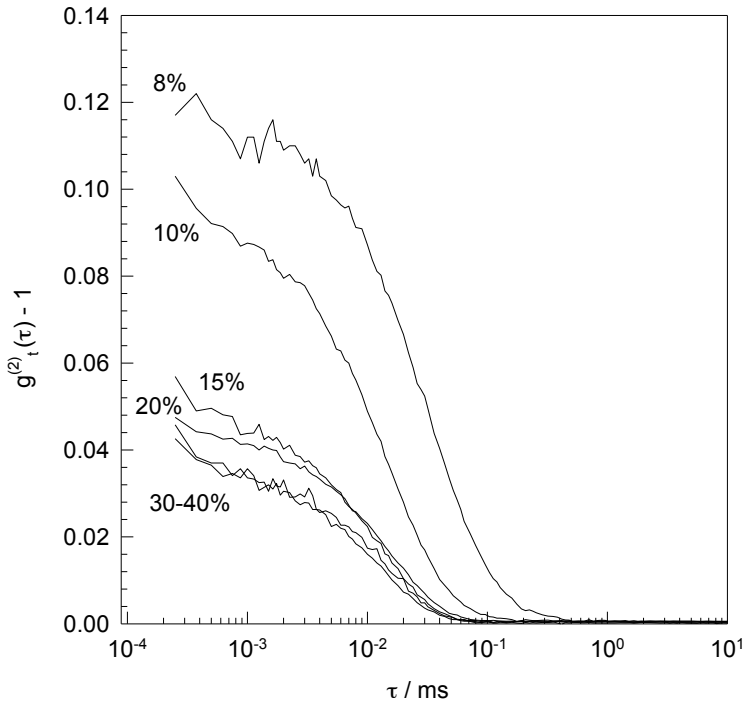

Figure 19. A Sample of intensity correlation curves for thiol-ene gels synthesized at different concentrations.

The ensemble scattering intensity from the gels has two components, i.e. static and dynamic, which originate from the frozen-in and the dynamic structure of the gels respectively [35,40,41] . The nonergodic approach, mentioned in section 3.1.1, is utilized to separate these two components with the help of equation 49.

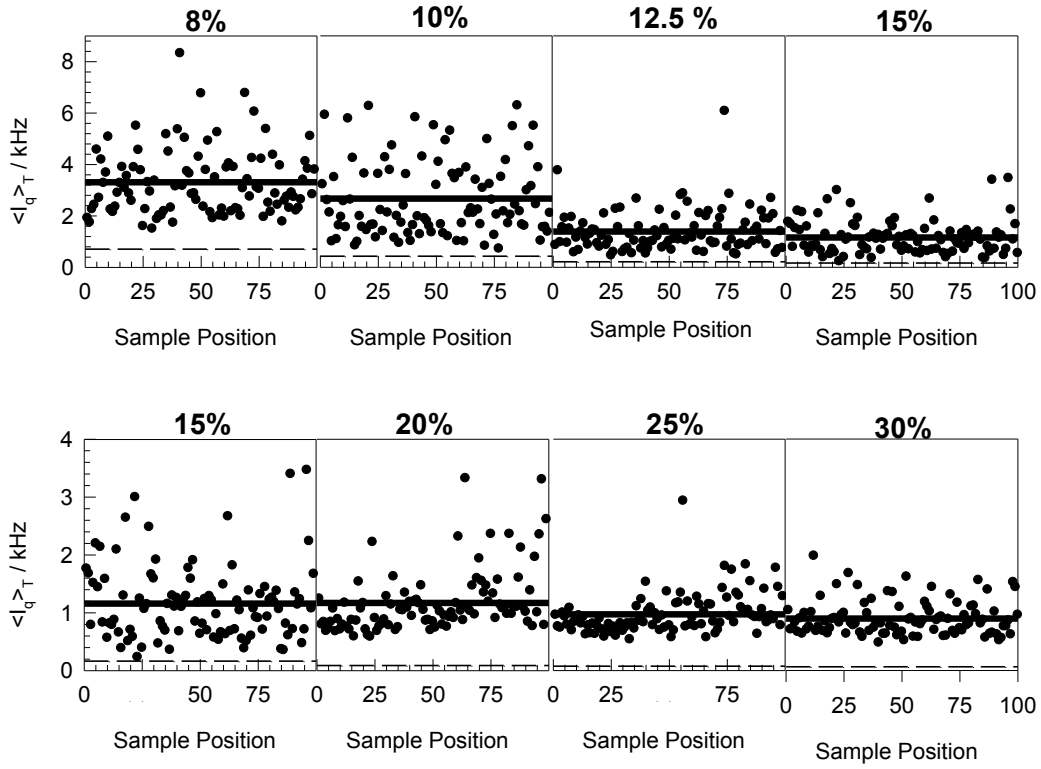

Figure 20. Variation of time averaged scattering intensity with sample position of thiol-ene organogels synthesized at different monomer concentrations before the solvent correction (see text). Solid and dashed lines represent the ensemble-averaged scattered intensity, $\langle I \rangle_E$, and the fluctuating component of the scattering intensity, $\langle I \rangle_F$, respectively.

Figure 20 shows the speckle pattern formed after 100 measurements performed at different sample positions of the time averaged scattering intensities. Calculated $\langle I \rangle_F$ values do not seem to match with the data on the plots for the concentrations 20% and higher where data points close to $\langle I \rangle_F$ are not observed. This is thought to be due to the incoherent contribution of the solvent scattering to the total scattering intensity. As mentioned in the discussion of Figure 9, the scattering intensity of the resultant thiol-ene networks are not more than twice the scattering value of unreacted reaction mixture at the same composition. This means the scattering intensities of the thiol-ene networks studied are in the range of the pure solvent and this incoherent solvent scattering is quite likely to heterodyne and affect the calculated results [62]. As the value of scattering from the pure solvent is measured it is found to be 0.456 kHz, which is almost half of the magnitude of

the ensemble average scattering intensity from the sample at 30% polymer concentration.

In order to prevent the error that originates from the solvent scattering, we simply subtracted the solvent scattering intensity from the $\langle I \rangle_E$ and $\langle I \rangle_T$ values of every single measurement and recalculated the $\langle I \rangle_F$ values. The results are shown in Figure 21. As shown in the figure, an exact match between $\langle I \rangle_F$ and smallest $\langle I \rangle_T$ values is obtained when the solvent scattering is subtracted.

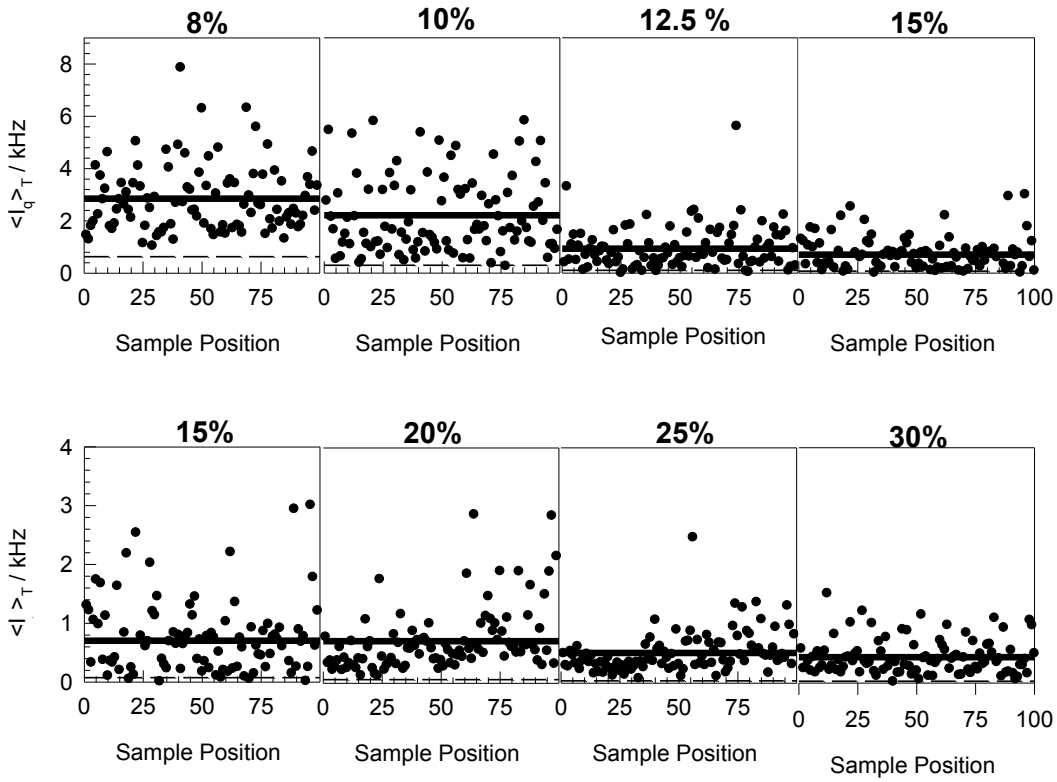

Figure 21. Variation of time averaged scattering intensity with sample position of thiol-ene organogels synthesized at different monomer concentrations after the solvent correction. Solid and dashed lines represent the ensemble-averaged scattered intensity, $\langle I \rangle_E$, and fluctuating component of the scattering intensity, $\langle I \rangle_F$, respectively.

The time average scattering intensities of the gels show a strong dependence on sample position. However, the ensemble average scattering intensity decreases with increasing monomer concentration, which can be explained by considering the reduction of the concentration difference between densely and loosely crosslinked regions with increasing monomer concentration.

Nevertheless, despite the very small values of the intensities of the scattered light, it would not be correct to state that these gels are homogenous.

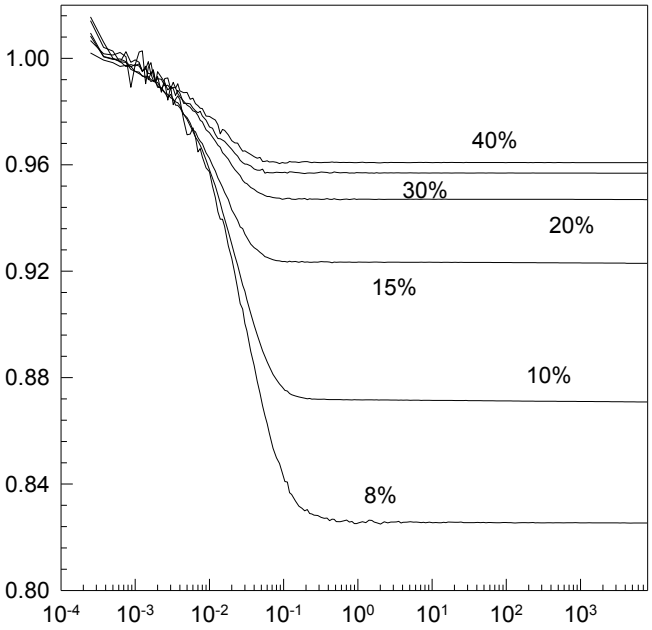

Figure 22. An example of normalized intermediate scattering functions calculated for thiol-ene gels synthesized at different monomer concentrations.

The nonergodic approach is applied in order to separate scattering from dynamic fluctuations and frozen-in structures inside the network. The curves in Figure 22 are calculated as the normalized intermediate scattering functions from the autocorrelation functions shown in Figure 19 by using equation 49. Then the curves were fitted to equation 20. The amount of decay, *A,* and the height of the plateau region, $f(q,\infty)$, of the curves represent the fractions of dynamic contribution and from the frozen-in structure to the ensemble average scattering intensity, respectively. It is clear in the figure that the dynamic portion of the scattering decreases with increasing total monomer concentration.

In Figure 23 the average values of the ratio of the ensemble average scattering intensity and the contribution of dynamic fluctuations in the gel, $\langle I \rangle_F / \langle I \rangle_E$, obtained by the nonergodic approach, is plotted. Calculations show that only a quite small portion of the total scattering intensity originates from the dynamic fluctuations within the gel networks. Especially for the

concentrations above 15 %, the contribution of dynamic fluctuations to the ensemble average scattering intensity is below 10%, which means most of the gel network is composed of frozen-in structures.

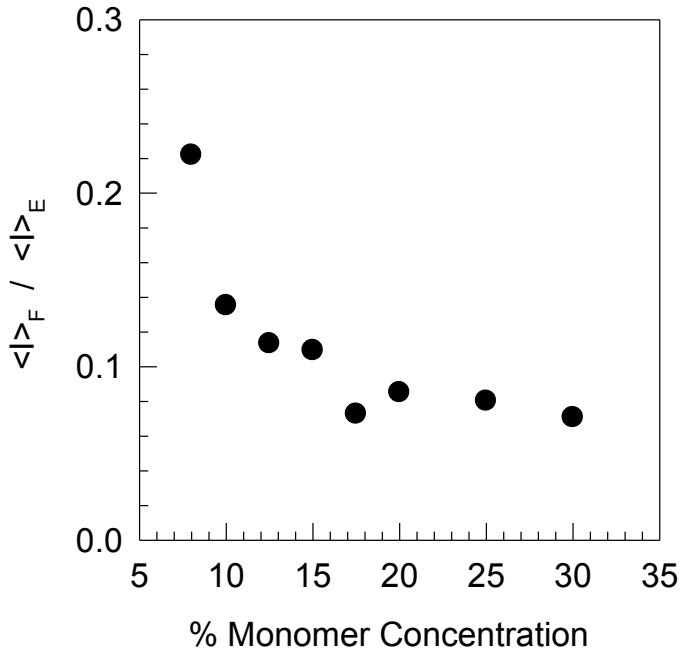

Figure 23. The ratio of fluctuating component of the scattering to the ensemble average scattering intensity ($\langle I \rangle_F / \langle I \rangle_E$) of thiol-ene organogels synthesized at different monomer concentrations.

Since thiol-ene polymerization proceeds via a step-growth mechanism and no homopolymerization occurs with the TEGDVE monomer a relatively ordered and homogeneous structure is expected to be formed. Also, without homopolymerization the chain length between the cross-links would be rather short, which is expected to lead high moduli for the gels. By considering these facts it is expected to obtain a quite stiff network with a very low portion of dynamic structure inside. So, having more than 90% static contribution to the ensemble scattering intensity does not necessarily mean that the structure is inhomogeneous. However the measurements carried out with the gels in equilibrium swollen state are a good indicator for the characterization of the inhomogeneity of the corresponding gels. Figure 24 shows the DLS measurements carried out with gel samples just after synthesis and in the equilibrium swollen states. The graphs have been drawn to the same scale to facilitate comparison. The data for the right after synthesis state is shown in a

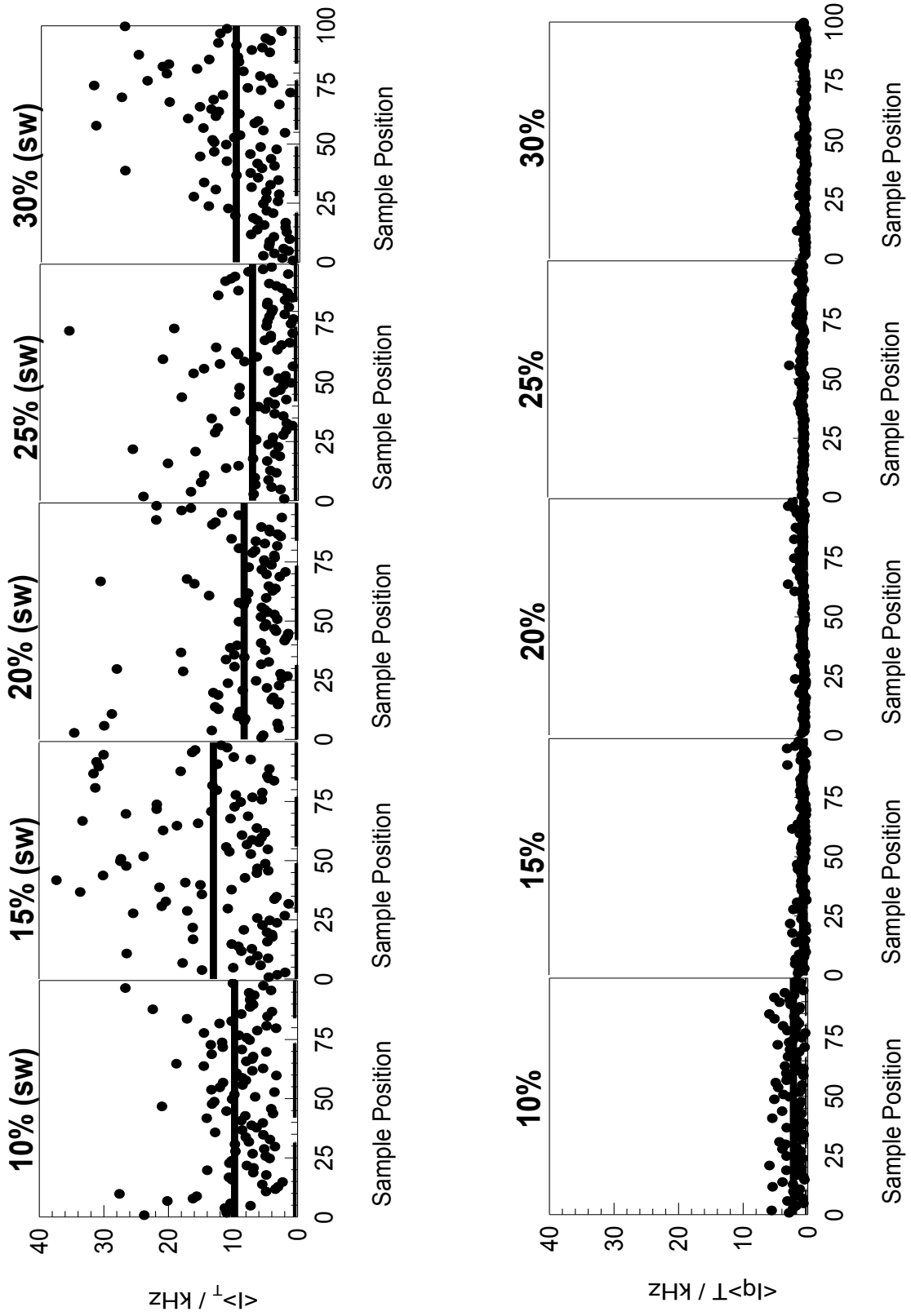

Figure 24. Variation of time averaged scattering intensities with sample position of thiol-ene organogels synthesized at different monomer concentrations, at their right after synthesis and equilibrium swollen states. Solid and dashed lines represent the ensemble-averaged scattered intensity, and the fluctuating component of the scattering intensity, respectively.

greater detail in Figure 21. As can be seen from the figure, swelling process causes a dramatic increase in the scattering intensity of the thiol-ene organogels. This behavior, actually, reveals the inhomogenous microstructure of the corresponding network. It is known that the crosslink density fluctuations inside the gel may not always be detectable by scattering methods right after the synthesis due to the high polymer concentration but become visible with swelling of the network, since the densely crosslinked regions swell much less than the loosely crosslinked regions [37,64]. Hence, most of the swelling process is achieved by those loosely crosslinked regions. This natural difference between densely and loosely crosslinked regions reveals the inhomogenous crosslinking by increasing the contrast inside the gel and increasing the ensemble average scattering intensity which is the exact case exhibited in Figure 24. As can be seen from the figure, the ensemble average scattering intensity is no more concentration dependent after the gels are in their equilibrium swollen states. This suggests that the decrease of $\langle I \rangle_E$ with increasing concentration that is observed right after the synthesis is not due to the homogenous structure of the gels but rather due to the space filling effect of the polymer, which covers the inhomogeneous crosslinking character of the reaction itself.

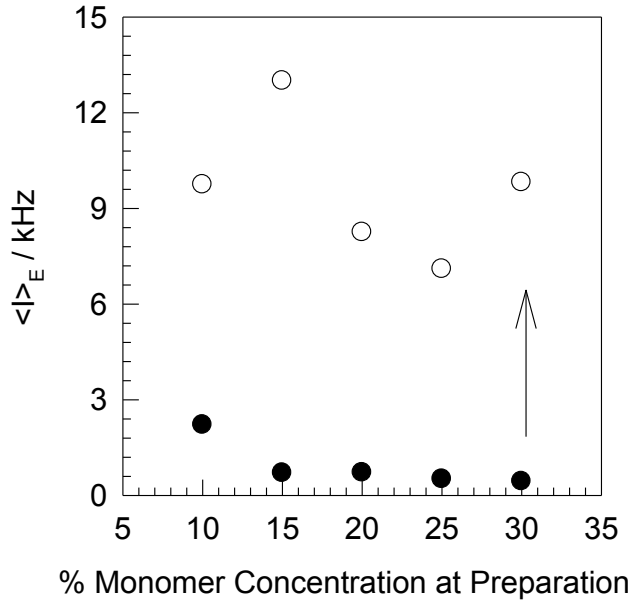

Figure 25. Ensemble average scattering intensity of the thiol-ene organogels synthesized at different monomer concentrations. Filled and open symbols represent right after synthesis and the equilibrium swollen states, respectively.

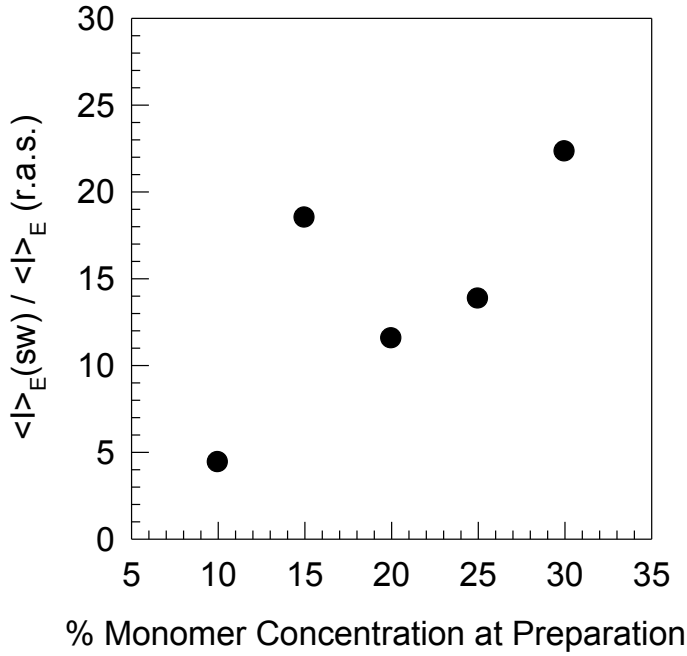

Figure 26. The ratio of the ensemble average scattering intensities of the thiol-ene organogels at right after synthesis and equilibrium swollen states at different monomer concentrations employed for synthesis.

Figures 25 and 26 are plotted in order to underline the variation of the ensemble average scattering intensity with swelling. As can be seen from the figures, the values of ensemble average scattering intensity show no significant concentration dependence and increase up to 25 fold by equilibrium swelling compared to ones at the right after synthesis states.

As the dynamic contribution to the ensemble average scattering intensity is calculated (Figure 27 and 28) the $\langle I \rangle_F$ is found to be increased slightly, due to the separation of the polymer chains by swelling, which provides the chains more space to fluctuate. However, the fraction of dynamic contribution to the ensemble average scattering intensity, $\langle I \rangle_F / \langle I \rangle_E$ values are found to be decreased. This result actually underlines the static nature of the thiol-ene networks studied and implies that there is no significant physical entanglements in the network structure. Increasing $\langle I \rangle_F$ values of swollen samples at 25 and 30% monomer concentrations are due to the experimental error, while the values are too small.

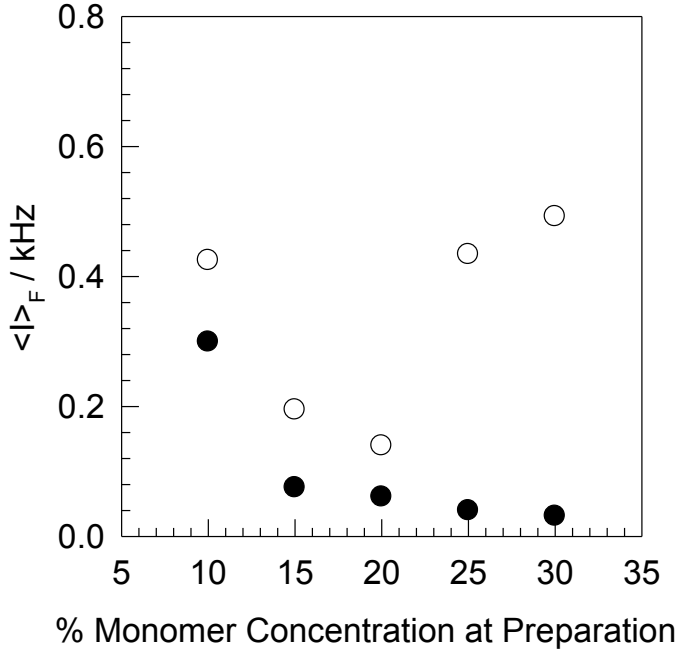

Figure 27. Fluctuating component of the total scattering intensity of thiol-ene organogels synthesized at different monomer concentrations. Filled and open symbols represent right after synthesis and the equilibrium swollen states respectively

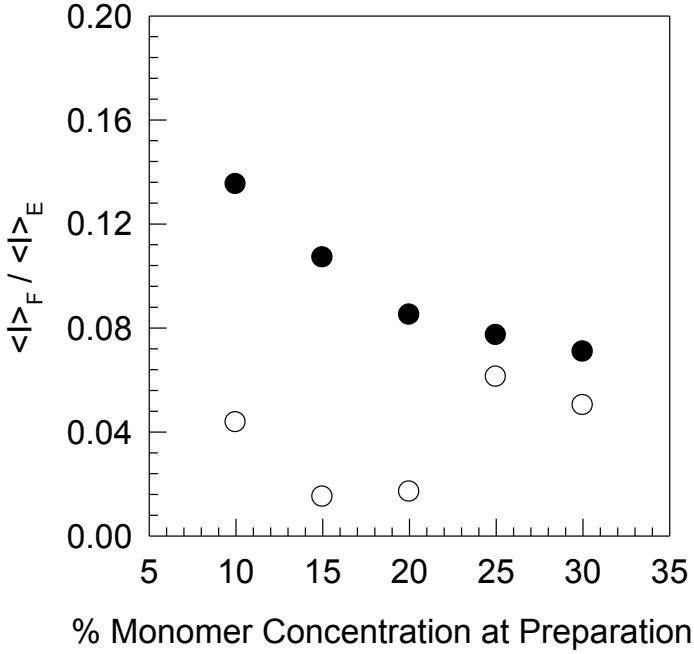

Figure 28. The ratio of fluctuating component of the scattering to the ensemble average scattering intensity ($\langle I \rangle_F / \langle I \rangle_E$) at different monomer concentrations. Filled and open symbols represent right after synthesis and the equilibrium swollen states respectively.

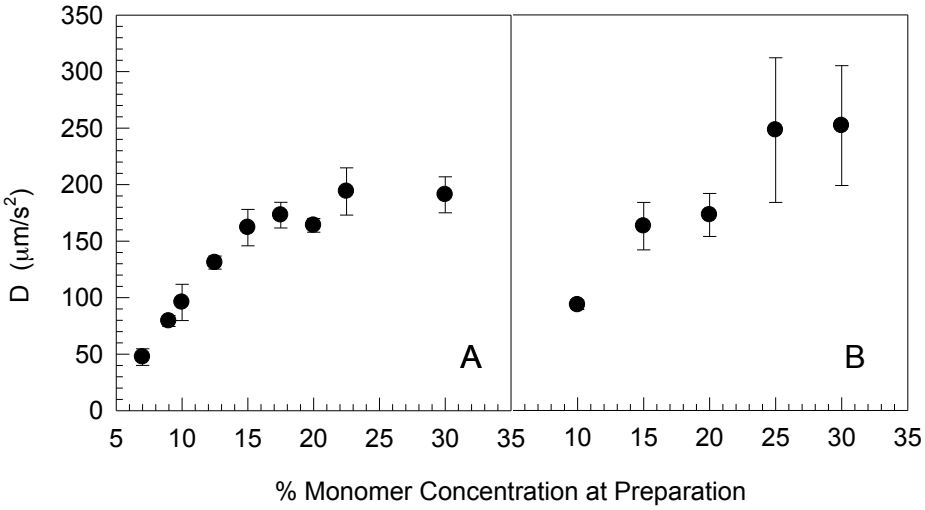

Figure 29. Cooperative diffusion coefficients of thiol-ene networks in (A) right after synthesis and (B) equilibrium swollen states.

Calculated cooperative diffusion coefficients are given in Figure 29. Plot A and B show the diffusion coefficients of the gels in right after synthesis and equilibrium swollen states. Plotted data points are the mean values of 15 measurements. As can be seen from the plots, the diffusion coefficients of the gels increase with increasing monomer concentration up to 17.5% and stays constant which is an indication of fixed distance between crosslink points. With further swelling no significant change is observed on the mean values of diffusion coefficients but the standard deviation from the average values increase significantly, especially for the concentrations above 20% which reflects the existance of densely and loosely crosslinked regions, and hence, the inhomogeneous structure of the networks.

6 SUMMARY AND CONCLUSION

Within the context of this study thiol-ene networks were synthesized at different concentrations by using a difunctional ene monomer and a tetrafunctional thiol crosslinker. The studied network is thought to have a homogenous structure due to the stepgrowth nature of the polymerization mechanism during synthesis. The aim of this thesis was to investigate this phenomena with the help of direct methods such as rheology and dynamic light scattering. Gelation characteristics and the microstructure of the resultant networks are investigated.

Rheological measurements conducted during and after the synthesis of thiol-ene networks showed that the gelation reaction via thiol-ene mechanism is quite rapid. Syneresis is observed for the networks below 20% monomer concentration since the network contracts as the clusters merge during the crosslinking reaction. Crosslink density is found to increase up to 40% monomer concentration and then stays almost constant due to the steric hindrance and decreased mobility of the network chains. However, a relatively high crosslinking efficiency up to 60% for phantom network model is calculated and explained by the high monomer conversion which is above 70%, at the gel point.

On the other hand, DLS measurements conducted with networks right after synthesis have quite small light scattering intensity values, i.e., smaller than twice the value of solvent scattering intensity. Thus incoherent solvent scattering was found to interfere with the scattering of the networks studied. When the data were analysed with the nonergodic approach, it has been realized that a solvent correction was necessary. In order to correct the data, solvent scattering intensity value was simply subtracted from the total scattering intensity and the analysis was performed with the network scattering intensity values.

When the data were analyzed with the help of the nonergodic approach, the static portion of the ensemble scattering intensity is calculated as 90±2% for concentrations 10% and above, which suggests an inhomogeneous microstructure. Since the monomers do not homopolymerize, the network

formed with short TEGDVE monomer chains between PETMP units were expected to result in a rigid, homogenous structure. However, as DLS mesurements were carried out with gels in their equilibrium swollen state, the ensemble average scattering intensity is found to increase up to 25 fold relative to the samples at the right-after-synthesis states, which uncovers the inhomogenous nature of the thiol-ene networks despite the high crosslinking efficiency.

It is noteworthy that the ensemle average scattering intensities for thiol-ene networks at equilibrium swollen state are not concentration dependent and show no pattern, which suggests that the microstructure of equilibrium swollen gels are similar.

Also, the calculated cooperative diffusion coefficients of studied networks at the right after synthesis and equilibrium swollen states reflects the inhomogeneous structure of thiol-ene networks. Actually, the mean values of cooperative diffusion coefficients do not show a significant difference with swelling. However, standard deviations of the mean values of the cooperative diffusion coefficients increase abrubtly, which is explained by the inhomogeneous swelling process inside the network, resulting in an increased contrast of highly and loosely crosslinked regions.

7 REFERENCES

1. Nguyen K., West J., *Biomaterials*, 2002, 23, 4307.
2. Peppas N.A., *Curr. Opin. Coll. Int. Sci.,* 1997, 2, 531-537.
3. Richter A., Türke A., Pich A., *Adv. Mater.,* 2007, 19, 1109-1112.
4. Eddington D.T., Beebe D.J., *Adv. Drug Delivery Rev.*, 2004, 56,199-210.
5. Kabiri K., Zohuriaan-Mehr M.J., *Polym. Adv. Tech.,* 2003, 14, 348-444.
6. Hennink W.E., Nostrum C.F., *Adv. Drug Deliv. Rev.,* 2002, 54, 13-36.
7. Akay G., Hassan-Raeisi A., Tuncaboylu D.C., Orakdogen N., Abdurrahmanoglu S., Oppermann W., Okay O., *Soft Matter.,* 9, 2254-2261.
8. Ide N., Fukuda T., *Macromolecules,* 1999, *32*, 95-99.
9. Kuru E.A., Okay O., *Eur. Polym. J.,* 2007, 43, 2913-2921.
10. Susoff M., Oppermann W., *Macromolecules,* 2009, 42, 9195-9198.
11. Hoyle C.E., Lee T.Y., Roper T., *J. Polym. Sci. Part A: Polym. Chem.,* 2004, 4, 5301-5338.
12. Senyurt A.F., Wei H., Hoyle C.E., Pilland S.G., Gould T.E., *Macromolecules,* 2007, 40, 4901-4909.
13. Senyurt A.F., Wei H., Phillips B., Cole M., Nazarenko S., Hoyle C.E. Piland S.G., Gould T.E., *Macromolecules,* 2006, 39, 6315-6317.
14. Kade M.J., Burke D.J., Hawker C.J., *J. Polym. Sci. Part A: Polym. Chem.,* 2010, 48, 743-750.
15. Carraher Jr. C.E., *Seymour/Carrahers's Polymer Chemistry,* 7th Ed., 2007, CRC Press, pp.90-92.
16. Posner T., *Berichte der Deutschen Chemischen Gesellschaft,* 1905, 38, 646.
17. Karasch M.S., Mayo F.R., *Chem. Ind.,* 1938, 57, 752.
18. Khire V.S., Lee T.Y., Bowman C.N., *Macromolecules,* 2007, 40, 5669–5677.
19. Boulden J.E., Cramer N.B., Schreck K.M., Couch C.L., Bracho-Troconis C., Stansbury J.W., Bowman C.N., *Dental Mater.,* 2011, 3, 267-272.

20. Sikanen T.M., Lafleur J.P., Moilanen, M.E., Zhuang G.S., Jensen T.G., Kutter J.P., *J. Micromech. Microeng.,* 2013, 23, 037002.
21. Ma X.P., Zhou Z.X.; Jin E.L., Sun Q.H., Zhang B., Tang J.B., Shen Y.Q., *Macromolecules,* 2013, 46, 37-42.
22. Temel G., Karaca N., Arsu N., *J. Polym. Sci. Part A: Polym. Chem.,* 2010, 48, 5306-5312.
23. Cramer N.B., Scott J.P., Bowman C.N., *Macromolecules,* 2002, 35, 5361-5365.
24. Cook W.D., Chen F., Pattison D.W., Hopson P., Beaujon M., *Polym. Int.,* 2007, 56, 1572.
25. Cole M.A., Jankousky K.C., Bowman C.N., *Polym. Chem.,* 2013, 4, 1167
26. D'Souza V.T., Nanjundiah R., Baeza H.J., Szmant H.H., *J. Org. Chem.,* 1987, 52, 1720.
27. Sensfuß S., Friedrich M., Klemm E., *Makromol. Chem.,* 1991, 192, 2895.
28. Andrejewska E., Zych-Tomkowiak D., Andrejewski M., Hug G.L., Marciniak B., *Macromolecules,* 2006, 39, 3777
29. Bibaut-Renauld C., Burget D., Fouasier J.P., Varelas C.G., Thomatos J., Tsagaropoulos G. Ryrfors L.O., Karlsson O.J., *J. Polym. Sci. Part A: Polym. Chem.,* 2002, 40, 6171-6181.
30. Jiang S., Xia K.-Q., Xu G., *Macromolecules,* 2001, 34, 7783.
31. Kanao M., Matsuda Y., Sato T., *Macromolecules,* 2003, 36, 2093.
32. Aymard P., Durand D., Nicolai T., *Int. J. Polym. Anal. Charact.,* 1996, 2, 115.
33. Gimel J.C., Durand D., Nicolai T., *Macromolecules,* 1994, 25, 583.
34. Papadakis C.M., Almdal K., Mortensen K., Rittig F., Fleischer G., Stepanek P., *Eur. Phys. J.,* E 2000, 275.
35. Pusey P.N., Van Megen W., *Physica A,* 1989, 157, 705-741.
36. Rouf-George C., Munch J.P., Schosseler F., Pouchelon A., Beinert G., Boue F., Bastide J., *Macromolecules,* 1997, 30,8344.
37. Shibayama M., *Macromol. Chem. Phys.* 1998, 199, 1-30.
38. Zhao Y., Zhang G., Wu C., *Macromolecules,* 2001, 34, 7404.

39. Hecht A.M., Horkay F.H., Schleger P., Geissler E., *Macromolecules,* 2002, 35, 8552.
40. Nie J., Du B., Oppermann W., *J. Phys. Chem. B,* 2006, 110, 11167-11175.
41. Miyazaki S., Endo H., Karino T., Haraguchi K., Shibayama M., *Macromolecules,* 2007, 40, 4287-4295.
42. Berne B.J., Pecora R., *Dynamic Light Scattering With Applications to Chemistry, Biology, and Physics*, 1976, John Wiley & Sons, Inc.
43. Rubinstein M., Colby R.H., *Polymer Physics,* 2003, Oxford University Press, pp.345 .
44. Joosten J.G.H., Gelade E.T.F., Pusey P.N., *Physical Review A,* 1990 , 42, 2161-2175.
45. Shibayama M., Norisuye T., *Bull. Chem. Soc. Jpn.,* 2002, 75, 641-659.
46. Rubinstein M., Colby R.H., *Polymer Physics,* 2003, Oxford University Press, pp. 282.
47. Barnes H. A., *An Introduction to Rheology,* 1989, Elsevier, New York.
48. Ferry J.D., *Viscoelastic Properties of Polymers,* 1980, John Wiley & Sons Inc.
49. Rubinstein M., Colby R.H., *Polymer Physics,* 2003, Oxford University Press, pp. 255.
50. Ward I.M., Sweeney J., *An Introduction to Mecanical Properties of Solid Polymers,* 2nd Ed., 2004, John Wiley & Sons Inc.
51. Treolar L.R.G., *The Physics of Rubber Elasticity,* 3rd Ed., 1975, Clarendon Press, Oxford.
52. Anseth K.S., Bowman C.N., Peppas L.B., *Biomaterials,* 1996, 17, 1647-1657.
53. Hild G., *Prog. Polym. Sci.,* 1998, 23, 1019-1149.
54. Mark J.E., Erman B., *Rubberlike Elasticity- A Molecular Primer,* 1988, John Wiley & Sons Inc., pp. 26.
55. Erman B., Mark J.E., *Annu. Rev. Phys. Chem.,* 1989, 40, 351-374.
56. Flory P.J., *Principles of Polymer Chemistry,* 1953, Cornell University Press, Ithaca, New York.
57. Flory P.J., Rehner J., *J. Chem. Phys.,* 1943, 11, 521-527
58. Flory P.J., *J. Chem. Phys.,* 1942, 10, 51-61.

59. Huggins M.L., *J. Chem. Phys.,* 1942, 46, 151-158
60. Ricka J., *Habilitation Thesis: Fluctuations and Correlations: Dynamic Light Scattering*, 1994, Unknown.
61. Flammer I., Ricka J., *Applied Optics,* 1997, 36, 7508-7517.
62. Duskova-Smrckova M., Valentova H., Durackova A., Dusek K., *Macromolecules,* 2010, 43, 6450-6462.
63. Dusek K., Duskova-Smrckova M., *Prog. Polym. Sci.,* 2000, 25, 1215-1260.
64. Kizilay M.Y., Okay O., *Polymer,* 45, 8, 2567-2576.

APPENDIX A - List of Chemicals

Substance	Abbreviation	Molar Mass (g/mol)	Supplier	Purity
Pentaerithritol tetrakis(3-mercaptopropionate)	PETMP	488	donated by Bruno Bock Chemische Fabrik GmbH&Co. Kg	>95%
Triethyleneglycol divinylether	TEGDVE	202	Sigma-Aldrich	>98%
Camphorquinone	CQ	166.22	Sigma-Aldrich	>97%
1,1,2-Trichlorethane	TCE	133.4	Acros Organics	>98%

APPENDIX B – Molar Amounts of Chemicals Used in the Study

Chemical	7%	8%	9%	10%	12.5%	15%
PETMP	0.0785 M	0.0897 M	0.1009 M	0.1121 M	0.1401 M	0.1682 M
TEGDVE	0.1569 M	0.1794 M	0.2018 M	0.2242 M	0.2803 M	0.3363 M
CQ	1.21 mM	1.21 mM	1.21 mM	1.21 mM	1.21 mM	1.21 mM

Chemical	17.5%	20%	22.5%	25%	30%	35%
PETMP	0.1962 M	0.2242 M	0.2522 M	0.2802 M	0.3364 M	0.3924 M
TEGDVE	0.3924 M	0.4484 M	0.5045 M	0.5604 M	0.6728 M	0.7848 M
CQ	1.21 mM	1.21 mM	1.21 mM	1.21 mM	1.21 mM	1.21 mM

Chemical	40%	50%	60%	80%	100%
PETMP	0.4484 M	0.5604 M	0.6728 M	0.8968 M	1.2669 M
TEGDVE	0.8968 M	1.1208 M	1.3456 M	1.7936 M	2.5337 M
CQ	1.21 mM	1.21 mM	1.21 mM	1.21 mM	1.21 mM